Journal of Materials Chemistry B

ROYAL SOCIETY OF CHEMISTRY

PAPER

View Article Online
View Journal | View Issue

Cite this: J. Mater. Chem. B, 2026, 14, 6681

Dual-targeting sepsis-associated inflammation and infection using linoleic acid-based lipid–polymer hybrid nanoparticles

Abdelrahman Tageldin,[a] Calvin A. Omolo,[ab] Vincent O. Nyandoro,[ac] Mohammed A. Gafar,[ad] Eman A. Ismail,[ae] Lucy W. Kiruri,[f] Bongani B. Nkambule,[g] Irene Mackraj[g] and Thirumala Govender*[a]

Bacterial sepsis is a critical and life-threatening condition resulting from a dysregulated host immune response to infection and remains one of the foremost causes of mortality worldwide. In this study, a biomimetic hybrid lipid–polymer nanocarrier (VCM-LIN-P2O NPs) was designed to target the ADAM10 and TLR2 receptor pathways through integrating linoleic acid (LIN) and poly(2-ethyl-2-oxazoline) (P2O). This engineered nanoplatform attenuates excessive inflammation *via* concurrent binding to ADAM10 and TLR2 while ensuring targeted delivery of vancomycin (VCM) to infection sites. The potential of LIN to competitively bind to ADAM10 and TLR2 was initially examined through molecular docking and subsequently validated using microscale thermophoresis (MST), confirming the potential ability of LIN to downregulate the inflammation associated with ADAM10 and TLR2 activation. The optimized VCM-LIN-P2O NPs displayed desirable physicochemical characteristics, excellent biocompatibility, and high stability, along with a sustained drug release profile extending up to 48 hours. Furthermore, the nanocarrier exhibited enhanced *in vitro* antibacterial performance compared to bare VCM, along with significant antioxidant and anti-inflammatory activity, in LPS-stimulated macrophages. In a murine MRSA-induced sepsis model, treatment with VCM-LIN-P2O NPs resulted in marked bacterial clearance from major organs and the bloodstream, accompanied by a significant reduction in TNF-α, IL-1β, and IL-18 levels, thereby alleviating organ damage. Therefore, these findings establish VCM-LIN-P2O NPs as a promising multifunctional nanoplatform for targeted antibiotic delivery and effective sepsis therapy.

Received 26th January 2026,
Accepted 24th March 2026

DOI: 10.1039/d6tb00207b

rsc.li/materials-b

1. Introduction

Bacterial sepsis is a systemic condition resulting from a dysregulated immune response to bacterial invasion and is one of the leading causes of global mortality and morbidity, according to the World Health Organization (WHO).[1,2] Recent epidemiological data indicate that sepsis accounts for approximately 20% of all global deaths annually.[3] Although antibiotics remain the primary treatment for sepsis, the emergence of antimicrobial resistance, coupled with a decline in the development of new antibiotics, pose a serious challenge to effective management.[4] Moreover, the complex pathophysiology of sepsis often necessitates the use of multiple adjunctive therapies, beyond antibiotics, to control inflammation and mitigate oxidative stress-induced organ damage, potentially reducing patient compliance.[5,6] Consequently, there is an urgent need for more effective and multimodal therapeutic strategies to enhance the treatment outcomes of sepsis.

Recent advances in nanotechnology have significantly enhanced therapeutic outcomes for various diseases, including bacterial infections and sepsis.[5,7] Nanocarriers with well-optimized physicochemical characteristics have addressed many limitations associated with conventional drug delivery systems, such as enhancing the solubility of hydrophobic drugs, enabling prolonged systemic circulation, and promoting selective accumulation at infection sites.[6,8] Nevertheless,

[a] Discipline of Pharmaceutical Sciences, College of Health Sciences, University of KwaZulu-Natal, Private Bag X54001, Durban, South Africa. E-mail: comolo@usiu.ac.ke, Govenderth@ukzn.ac.za
[b] School of Pharmacy and Health Sciences, Department of Pharmaceutics, United States International University-Africa, P. O. Box 14634-00800, Nairobi, Kenya
[c] Department of Pharmaceutical Chemistry and Pharmaceutics, School of Pharmacy, Kabarak University, P.O. BOX Private bag 20157, Nakuru, Kenya
[d] Department of Pharmaceutics, Faculty of Pharmacy, University of Khartoum, P.O. Box 1996, Khartoum, Sudan
[e] Department of Pharmaceutics, Faculty of Pharmacy, University of Gezira, Wad Madani, Sudan
[f] Department of Chemistry, Kenyatta University, Nairobi, Kenya
[g] Discipline of Human Physiology, School of Laboratory Medicine and Medical Sciences, College of Health Sciences, University of KwaZulu-Natal, Durban, South Africa

several challenges remain unresolved, including inadequate target specificity, especially with complex diseases such as sepsis, which necessitates the use of biomimetic materials to target multiple pathways besides the invading pathogen, highlighting the need for continued research and innovation.[9]

Notably, the pathogenesis of bacterial sepsis is mediated through the activation of multiple immunopathological pathways. The sepsis microenvironment is also characterized by bacterial virulence factors, such as alpha-hemolysin, which facilitate persistent infection.[10] One promising strategy for attenuating sepsis associated with bacterial infection involves the design of multifunctional biomimetic nanocarriers that mimic natural substrates of overexpressed receptors and bacterial enzymes within the sepsis milieu. These bioinspired systems could provide dual functionality: targeted antibiotic delivery and modulation of the hyperinflammatory response.[11] However, research in this domain remains at an early stage, particularly in the context of bacterial infections and sepsis. Only a limited number of studies have explored the development of multifunctional biomimetic nanoparticles for targeted antibacterial therapy.[12–15] Therefore, this emerging field holds significant potential for advancing antibiotic delivery strategies against bacterial sepsis and addressing the global challenge of antimicrobial resistance.

For instance, toll-like receptor (TLR) signaling, particularly through TLR2, and A Disintegrin and Metalloprotease 10 (ADAM10), which contributes to the activation of the NOD-like receptor family pyrin domain-containing 3 (NLRP3) inflammasome, are among the key pathways involved in initiating the innate immune response against bacterial sepsis.[16–18] These pathways play a critical role in recognizing toxins released by bacteria, such as peptidoglycan (PGN) and alpha-hemolysin (α-H), thereby initiating a rapid immune response aimed at controlling the infection. However, during severe infections, dysregulated or excessive activation of these receptors contributes to systemic inflammation and multi-organ damage, exacerbating disease progression.[16–18] Modulation of these inflammatory pathways using biomimetic strategies represents a promising and innovative approach for the treatment of inflammatory diseases, such as sepsis.[11,12] A variety of synthetic and natural compounds have been investigated for their potential to inhibit TLR2 and ADAM10-mediated inflammatory responses.[19–21] However, to our knowledge, no biomimetic nanodrug delivery system (NDS) has yet been developed to specifically target the ADAM10 receptor for the modulation of inflammation associated with sepsis. Furthermore, there are no existing reports describing the simultaneous targeting of both TLR2 and ADAM10 signaling pathways in the context of bacterial infections or other inflammatory diseases. This dual-targeting approach holds significant promise for enhancing therapeutic outcomes by increasing the specificity and efficacy of nanocarrier-based interventions, particularly in the treatment of MRSA-induced sepsis and related inflammatory disorders.

Among the diverse NDS, hybrid lipid–polymer nanoparticles (HLPNs) have gained considerable attention as an advanced platform for drug delivery, particularly in the management of bacterial infections and associated inflammatory conditions.[22] The integration of lipid and polymer constituents within HLPNs offers enhanced drug encapsulation efficiency and structural stability, supporting the delivery of both hydrophilic and hydrophobic therapeutics.[23] Their structural versatility also facilitates the incorporation of biomimetic materials, rendering HLPNs suitable for applications in anticancer, antimicrobial, and gene therapy.[22–24] Recently, our research group engineered innovative biomimetic HLPNs composed of tannic acid and oleylamine for the targeted delivery of ciprofloxacin in the context of bacterial sepsis.[25] Despite these advancements, to our knowledge, no biomimetic HLPNs have been reported that concurrently target ADAM10 and TLR2 receptors, representing a novel strategy in sepsis therapy.

The identification and application of materials with intrinsic biomimetic properties capable of simultaneously targeting multiple disease pathways represent a promising strategy for the development of HLPNs. In this regard, linoleic acid (LIN), a polyunsaturated fatty acid known for its inherent antioxidant[26] and anti-inflammatory properties,[26–28] presents a promising candidate for the design of biomimetic HLPNs, although its precise anti-inflammatory mechanisms remain unclear. We hypothesize that LIN may mimic bacterial toxins, thereby competitively inhibiting ADAM10 and TLR2 signaling pathways, ultimately leading to the attenuation of sepsis-associated inflammation. Additionally, poly(2-ethyl-2-oxazoline) (P2O), an FDA-approved polymer, exhibits intrinsic antibacterial activity by mimicking host defense peptides.[29] Integrating the antibacterial properties of P2O with the multifunctional bioactivity of LIN within a biomimetic HLPNs system offers a novel and promising therapeutic approach for the treatment of bacterial infection and its associated sepsis.

Therefore, this study aimed to develop multifunctional biomimetic HLPNs specifically engineered to target the inflammatory cascade associated with bacterial sepsis by modulating TLR2 and ADAM10 and augmenting the antibacterial efficacy of the loaded antibiotic. The engineered HLPNs consist of a lipid–polymer matrix integrating LIN, a polyunsaturated fatty acid with well-established systemic anti-inflammatory and antioxidant properties, and P2O, a newly FDA-approved polymer exhibiting intrinsic antibacterial activity. This nanoplatform, designated as VCM-LIN-P2O NPs, is designed to enable targeted delivery of vancomycin free base (VCM) for the treatment of bacterial sepsis. VCM was selected as a model drug because, although it is the first-line antibiotic for treating MRSA infections, resistance to it has been reported.[30] We hypothesize that the nanosystem may inhibit TLR2 and ADAM10 activity, thereby attenuating the excessive inflammatory response characteristic of sepsis and offering a novel therapeutic approach. To the best of our knowledge, the combination of LIN and P2O in the formulation of HLPNs has not been previously reported for the treatment of any disease. The results of LIN binding affinity, assessed through molecular docking and *in vitro* validation, are presented alongside the formulation and optimization of VCM-LIN-P2O NPs. In addition, comprehensive *in vitro*

characterization, including antibacterial, antioxidant, and anti-inflammatory evaluations, followed by *in vivo* assessment of antisepsis efficacy, are also reported.

2. Materials and methods

2.1 Materials

Details of the materials used are provided in the SI.

2.2 Molecular docking

For this study, we obtained the X-ray crystal structures of ADAM10 [PDB ID: 6BE6], alpha-hemolysin (α-H) [PDB ID: 3ANZ], and Human TLR2 (PDB ID: 6NIG) from the RCSB Protein Data Bank.[31] In all cases, only chain A was used for efficient computational analysis. Biologically relevant metal cofactors (Zn in ADAM10) were retained, and water molecules were removed. Missing hydrogens were added using AutoDockTools-1.5.7 software, and partial charges were assigned using the Kollman method. The ligands peptidoglycan (PGN) (CID: 5462260), lipoteichoic acid (LTH) (CID: 137349712), and linoleic acid (LIN) (CID: 5280450) were retrieved from PubChem. The structures were then subjected to energy minimization using the MMFF94 force field, which employs the steepest descent algorithm using Avogadro 1.2.0.[32] Binding affinities and protein–ligand interactions were obtained using the AutoDock Vina v.1.2.0. For Human TLR2 Vina docking, the search box centers and sizes were set to (x, y, z) = 8, 11, 80, and (size_x, size_y, size_z) = 36, 41, and 46 Å; exhaustiveness = 32; num_modes = 20. For ADAM10-LIN docking, the setting was as follows; the search box centers and sizes were set to (x, y, z) = 31, 18, 35 and (size_x, size_y, size_z) = 22, 24, and 17 Å; exhaustiveness = 32; num_modes = 20. Protein–protein docking of ADAM10 (chain A, Zn-retaining) and the 3ANZ receptor was performed using HADDOCK v2.5-2025.08,[33,34] which involves three steps. First, there are random orientations of the proteins followed by energy minimizations to remove steric clashes. Secondly, a flexible refinement step follows using torsion-angle dynamics, and finally, optimization in explicit solvent to improve interface geometry and stability. For ADAM10, alanine (Ala331) and leucine (Leu328 and Leu330) residues and the ligand binding pocket of 3ANZ were mentioned as "active" residues involved in the intermolecular interaction, while "passive" residues were defined as residues surrounding the active ones before submitting the docking job. Only one cluster was selected from seven clusters obtained from the HADDOCK results based on the HADDOCK score, *Z*-score and lowest RMSD. Software's UCSF Chimera,[35] PyMOL,[36] and LigPlot+[37] were used to analyze the docked complexes.

2.3 *In vitro* binding to TLR2 and ADAM 10

To experimentally substantiate the molecular docking outcomes and confirm the proposed biomimetic mechanism, the binding affinity of LIN for the ADAM10 and TLR2 receptors was analyzed using microscale thermophoresis (MST) on a Monolith NT.115 system (NanoTemper Technologies, Germany). In this assay, alpha-hemolysin (α-H) was used as the physiological substrate for ADAM10, whereas peptidoglycan (PGN) and lipoteichoic acid (LTH) were employed as standard ligands for TLR2. Both ADAM10 and TLR2 proteins were fluorescently tagged with RED-NHS 2nd generation dye (NanoTemper Technologies, Germany) following the manufacturer's protocol, and adjusted to a working concentration of 50 nM in phosphate-buffered saline (0.1 M PBS, pH 7.4) containing 0.05% Tween 20. Serial two-fold dilutions of each ligand (10 μL per dilution) were prepared in the same buffer and mixed with an equal volume of labeled protein solution, followed by a brief 5 minute incubation. The mixtures were then loaded into premium-coated capillaries and analyzed at 25 °C under excitation and MST powers of 70% and 40%, respectively. Dissociation constants (K_d) were calculated using MO-Affinity Analysis Software (v2.1.3, NanoTemper Technologies, Germany). Each measurement was performed in triplicate to confirm reproducibility and accuracy.

2.4 Preparation of VCM-LIN-P2O NPs

VCM-LIN-P2O NPs were prepared using a modified nanoprecipitation method,[38] a widely employed technique for fabricating nanocarriers such as polymeric nanoparticles and previously reported for VCM encapsulation.[11] Briefly, predetermined amounts of VCM, P2O, and the selected surfactant were dissolved in 10 mL of Milli-Q water to form the aqueous phase. The organic phase was prepared by dissolving LIN in 2 mL of acetone. Under continuous stirring at 600 rpm, the organic phase containing LIN was added dropwise to the aqueous phase containing VCM (1 mg mL^{-1}). The resulting emulsion was stirred for 24 hours to ensure complete acetone evaporation. Blank formulations (LIN-P2O NPs) were obtained using the same procedure, excluding VCM. The nanoformulations were stored at 4 °C until further characterization. Furthermore, to optimize the stability of VCM-LIN-P2O NPs, different surfactants (Tween 80, Tween 20, Poloxamer 407, Poloxamer 188, and Span 20) were screened. Subsequently, formulation parameters, including lipid-to-surfactant ratio, drug-to-system mass ratio, and lipid-to-polymer mass ratio, were systematically evaluated. The optimal formulation, defined by the smallest particle size (PS), lowest polydispersity index (PDI), and the highest entrapment efficiency (EE%) and drug-loading capacity (DL% w/w), was selected for further studies. Each formulation batch was prepared in triplicate.

2.5 Physicochemical characterization of VCM-LIN-P2O NPs

2.5.1 Determination of particle size, polydispersity index, and zeta potential. The PS, PDI, and ZP of the prepared VCM-LIN-P2O NPs were characterized using dynamic light scattering (DLS). Measurements were carried out on a Zetasizer Nano ZS90 instrument (Malvern Instruments, UK) equipped with a 633 nm laser and a 173° backscattering detection system. Prior to analysis, each sample was suitably diluted with distilled water to prevent multiple scattering effects. All measurements were performed at 25 °C, and each sample was analyzed in triplicate to ensure accuracy and reproducibility.[19]

2.5.2 Surface morphology. The morphological characteristics of VCM-LIN-P2O NPs were examined using transmission

electron microscopy (TEM) (JEOL JEM-1010, Japan). Briefly, a drop of appropriately diluted formulation was placed onto a coated copper grid and allowed to dry at room temperature. The sample was then stained with 2% phosphotungstic acid for 1 min and imaged at an accelerating voltage of 75 kV to obtain TEM images.

2.5.3 Determination of entrapment efficiency (EE%) and drug loading capacity (DLC% w/w). The EE% and DLC% (w/w) of VCM incorporated into VCM-LIN-P2O NPs were analyzed using a combined centrifugation and ultrafiltration approach.[25] For this purpose, 2 mL of each nanoparticle suspension (containing 1 mg mL^{-1} of VCM) was placed in Amicon® Ultra-4 centrifugal filter devices (Millipore, USA) with a 10 kDa molecular weight cut-off membrane and centrifuged at 3000 rpm for 30 minutes. The amount of unentrapped VCM in the filtrate was determined through high-performance liquid chromatography (HPLC) (Shimadzu, Japan) fitted with a photodiode array (PDA) detector operating at 280 nm. Chromatographic analysis was carried out using a Gemini® 5 μm NX-C18 110 Å (250 × 4.6 mm) column. The mobile phase consisted of 0.1% trifluoroacetic acid in water and acetonitrile (15 : 85, v/v), delivered at a flow rate of 1 mL min^{-1} under low-pressure gradient conditions, with an injection volume of 100 μL. Quantification was based on a standard calibration curve generated from the regression equation $y = 16\,329x + 410.19$ with a correlation coefficient (R^2) of 0.999. Each analysis was performed in triplicate, and the EE% and DLC% values were derived using the respective standard equations:

$$\text{EE\%} = \frac{\text{Total weight of VCM} - \text{Weight of free VCM}}{\text{Total weight of VCM}} \times 100$$

$$\text{DLC\%} = \frac{\text{Total weight of VCM} - \text{Weight of free VCM}}{\text{Total weight of nanoparticles}} \times 100$$

2.5.4 Thermal profile. Differential scanning calorimetry (DSC) was carried out using a Shimadzu DSC-60 instrument (Shimadzu, Japan) to record the thermal profiles of P2O, PLX407, free VCM, trehalose, physical mixture, and lyophilized VCM-LIN-P2O NPs using a previously reported method.[19] Approximately 5 mg of each sample was accurately weighed into an aluminum pan, sealed with a crimping press, and subjected to heating from room temperature to 500 °C at a constant rate of 10 °C min^{-1} under a nitrogen atmosphere. An empty sealed aluminum pan was used as a reference.

2.6 *In vitro* biocompatibility

2.6.1 *In vitro* cytocompatibility. The cytocompatibility of the developed VCM-LIN-P2O NPs was assessed using the MTT assay in accordance with previous reported procedures.[9] RAW 264.7 murine macrophage-like cells, HEK 293 human embryonic kidney cells, and HepG2 human hepatocellular carcinoma cells were cultured in Dulbecco's modified Eagle medium (DMEM) supplemented with 2.5% HEPES buffer, 1% (v/v) penicillin–streptomycin, 1% L-glutamine, and 10% (v/v) fetal bovine serum. The cells were maintained at 37 °C in a humidified incubator under 5% CO_2, and the medium was refreshed every two days. Once optimal confluence was achieved, cells were seeded into 96-well plates and incubated for 24 hours to allow adhesion. Thereafter, the medium was replaced with the test formulations at different concentrations (20, 40, 60, 80, and 100 μg mL^{-1}). Following the exposure period, the formulations were removed, and 20 μL of MTT solution (5 mg mL^{-1} in PBS) together with 100 μL of fresh medium were added to each well. Cell viability was evaluated based on the mitochondrial enzyme-driven conversion of MTT to insoluble formazan crystals. After 4 hours of incubation, the medium was discarded, and the crystals were solubilized with 100 μL of DMSO. The absorbance was then measured at 570 nm using a microplate reader (Spectrostar Nano, Germany) following a 1 hour incubation. Untreated cells served as positive controls, while medium without cells served as negative controls. All experiments were performed in triplicate, and cell viability (%) was calculated using the equation below:

$$\%\ \text{Cell viability} = \frac{A_{570\text{nm}}\ \text{treated cells}}{A_{570\text{nm}}\ \text{untreated cells}} \times 100$$

2.6.2 *In vitro* hemocompatibility. The hemocompatibility of VCM-LIN-P2O NPs was evaluated using a modified protocol adapted from a previously established method.[19] Fresh sheep blood was collected and washed three times with sterile phosphate-buffered saline (PBS) by centrifugation at 4000 rpm for 15 minutes to isolate red blood cells (RBCs). Subsequently, 0.2 mL of the RBC suspension was mixed with 1.8 mL of VCM-LIN-P2O NPs dispersions prepared at different concentrations (0.02–0.1 mg mL^{-1} in PBS). Distilled water and PBS were used as positive and negative controls, respectively. The samples were incubated at 37 °C for 1 hour, followed by centrifugation at 3000 rpm for 10 minutes at 4 °C using an ultracentrifuge (Centurion Scientific, UK). The absorbance of the supernatant was then recorded at 540 nm using a UV-Vis spectrophotometer (SpectraMax M2, USA). All assays were performed in triplicate, and the percentage of hemolysis was determined using the following equation:

$$\%\ \text{Hemolytic activity} = 100 - \frac{\text{ABS} - \text{ABSo}}{\text{ABS}_{100} - \text{ABSo}}$$

where ABS is the absorbance of the sample, ABS_{100} is the absorbance of the positive control, and ABS_0 represents the absorbance of the negative control.

2.7 *In vitro* drug release profile and kinetic modeling

The *in vitro* release behavior of VCM from VCM-LIN-P2O NPs was investigated using a modified dialysis technique.[39] Concisely, 2 mL of either a VCM aqueous solution (1 mg mL^{-1}) or a nanoparticle suspension containing an equivalent VCM concentration was placed into cellulose dialysis membranes (molecular weight cut-off = 14 kDa). Each bag was immersed in 40 mL of phosphate-buffered saline (PBS, 0.1 M, pH 7.4) and maintained at 37 °C under constant agitation at 100 rpm in a thermostatic shaker. At predetermined time points, 3 mL of the

release medium was withdrawn and replaced with an equal volume of fresh PBS to sustain sink conditions. The amount of VCM released at each interval was quantified by HPLC following the same analytical conditions used for determining the entrapment efficiency. All experiments were carried out in triplicate. To characterize the release mechanism, the cumulative release data were fitted to various kinetic models (zero-order, first-order, Higuchi, Korsmeyer–Peppas, Hixson–Crowell, and Weibull) using the DDSolver Excel add-in.[40] The model exhibiting the highest correlation coefficient (R^2) and the lowest root mean square error (RMSE) was considered the best to describe the release kinetics.

2.8 Short-term physical stability

The short-term physical stability of the VCM-LIN-P2O NPs was examined for 90 days under two storage conditions (ambient temperature and 4 °C). Variations in visual characteristics, PS, PDI, and ZP were periodically recorded. Each analysis was carried out in triplicate.

2.9 *In vitro* antibacterial efficacy

2.9.1 Evaluation of minimum inhibitory concentration. The minimum inhibitory concentration (MIC) of bare VCM, the blank nanosystem, and VCM-LIN-P2O NPs was determined against both methicillin-sensitive and methicillin-resistant *Staphylococcus aureus* (SA and MRSA) using the broth microdilution method.[9,41] In brief, overnight cultures of SA and MRSA were adjusted in Mueller–Hinton broth (MHB) to a turbidity equivalent to the 0.5 McFarland standard, verified using a densitometer (DEN-1B McFarland, Latvia). These suspensions were subsequently diluted with MHB to yield a final bacterial density of 5×10^5 CFU mL^{-1}. Serial dilutions of the formulations and bare VCM were prepared in MHB within 96-well plates to a final volume of 100 μL, after which 100 μL of the bacterial inoculum was added to each well. The plates were incubated at 37 °C under agitation (100 rpm). At 24, 48, and 72 hours, aliquots from each well were spotted onto Mueller–Hinton agar (MHA) plates, which were further incubated at 37 °C for 24 hours to assess bacterial growth and determine MIC values. All experiments were conducted in triplicate.

2.9.2 Kinetics of bacterial killing. The time-kill kinetics of VCM-LIN-P2O NPs were investigated using a colony-counting method previously described in the literature.[42] Briefly, an overnight culture of MRSA was adjusted to a final bacterial density of 5×10^5 CFU mL^{-1} and subsequently treated with 5 × MIC of either bare VCM or VCM-LIN-P2O NPs. PBS was included as a negative control. The cultures were incubated in a shaker incubator at 37 °C with agitation at 100 rpm for 24 hours. At specified time intervals, 0.1 mL aliquots were withdrawn, serially diluted, and plated onto MHA plates. The plates were incubated at 37 °C for an additional 24 hours, after which colony counts were recorded. All experiments were carried out in triplicate, and the results were expressed as logarithmic ($\log_{10}$) CFU mL^{-1} values.

2.9.3 MRSA cell membrane disruption. The membrane-disruptive effects of VCM-LIN-P2O NPs in comparison to bare VCM were examined using TEM based on a previously reported methodology.[9] Briefly, MRSA suspensions prepared in PBS at a density of 1.5×10^8 CFU mL^{-1} were combined in a 1 : 1 volume ratio with either bare VCM or VCM-LIN-P2O NPs, each applied at 10-fold their MIC. The mixtures were incubated at 37 °C for 2–4 hours under shaking conditions. Following incubation, aliquots were placed onto copper grids and examined using a JEOL JEM-1010 TEM (Japan) under brightfield, darkfield, and scanning transmission electron microscopy (STEM) diffraction modes.

2.10 *In vitro* antioxidant activity

2.10.1 DPPH scavenging activity. The antioxidant potential of LIN, P2O, and VCM-LIN-P2O NPs was assessed using a modified version of a previously reported DPPH assay.[19] A 0.5 mM solution of DPPH in methanol was freshly prepared, while LIN and P2O were dissolved at 2 mg mL^{-1}, corresponding to their concentrations in the VCM-LIN-P2O NPs formulation. Subsequently, 1.5 mL of each test solution was mixed with an equal volume of the DPPH solution and incubated in the dark at 37 °C. DPPH solution alone was used as the negative control, whereas ascorbic acid served as the positive control. After 1 hour of incubation, the absorbance of each reaction mixture was measured at 517 nm using a UV-vis spectrophotometer (SpectraMax M2, USA). All experiments were performed in triplicate, and the antioxidant activity was expressed as a percentage, calculated using the following formula:

$$\%\ \text{DPPH radical scavenging} = \frac{A_{517\ \text{control}} - A_{517\ \text{sample}}}{A_{517\ \text{control}}} \times 100$$

2.10.2 ROS scavenging at the mitochondrial level. RAW 264.7 cells were employed to evaluate the mitochondrial reactive oxygen species (ROS) scavenging capacity of VCM-LIN-P2O NPs, following the method reported by Zhan *et al.* (2019) with minor modifications.[43] Briefly, the cells were cultured as outlined in Section 2.5.1 and subsequently seeded onto coverslips placed in six-well plates at a density of 7×10^5 cells per well, followed by a 24 hours incubation. To stimulate an inflammatory response, the cells were pre-treated with lipopolysaccharide (LPS) at a concentration of 1 μg mL^{-1},[44] which represented the highest concentration that maintained cell viability above 90% for 4 hours, as shown in Fig. S5. Thereafter, they were exposed to the nanoparticle formulation (100 μg mL^{-1}) for an additional 14 hours. After treatment, the cells were rinsed three times with PBS and incubated with MitoSOX™ Red (2.5 μM; Thermo Fisher Scientific, USA), a mitochondrial superoxide indicator, for 20 minutes in the dark. Fluorescence signals were then examined using a fluorescence microscope.

2.11 *In vitro* anti-inflammatory activity

To further investigate the anti-inflammatory potential of VCM-LIN-P2O NPs, an *in vitro* model using the RAW 264.7 cell line was established, based on the protocol of Zhan *et al.* (2021), with minor modifications.[44] As outlined in Section 2.5.1, cells were cultured and subsequently seeded into 96-well plates at a

density of 5×10^3 cells per well, followed by a 24 hours incubation. To induce an inflammatory response, the cells were pretreated with LPS (1 μg mL^{-1}) for 4 hours. After stimulation, the cells were exposed to either VCM-LIN-P2O NPs (100 μg mL^{-1}) or bare VCM for 14 hours. The supernatants were then collected and assessed for pro-inflammatory cytokines, specifically tumor necrosis factor-alpha (TNF-α) and interleukin-1β (IL-1β), using ELISA kits in accordance with the manufacturer's instructions.

2.12 VCM-LIN-P2O NPs *in vivo* efficacy against the MRSA-induced sepsis in a mice model

2.12.1 Bacterial culture. *Staphylococcus aureus* Rosenbach (ATCC® BAA-70069™), a methicillin-resistant strain (MRSA), was grown in nutrient broth at 37 °C for 24 hours. The resulting culture was subsequently diluted in MHB, and its turbidity was standardized using a densitometer to achieve a final bacterial concentration of 5.0×10^9 CFU mL^{-1}.

2.12.2 Sepsis model in mice induced by MRSA infection. An *in vivo* experiment was performed using a BALB/c mice model of MRSA-induced sepsis to evaluate the preclinical therapeutic efficacy of VCM-LIN-P2O NPs. This sepsis model had been previously optimized and verified by our research group[11,42] and received ethical approval from the Animal Research Ethics Committee of the University of KwaZulu-Natal (approval number: AREC/00003417/2021). Male BALB/c mice weighing between 25 and 30 g were sourced from the Biomedical Resource Unit at the UKZN Westville Campus and accommodated in Type III cages under standardized laboratory conditions. Randomization was carried out by first weighing the animals and distributing them so that each group included the full range of body weights, and then randomly assigning treatments to reduce selection bias. The animals were randomly divided into four groups. Each group contains 6 animals: (i) uninfected controls administered PBS, (ii) MRSA-infected controls treated with PBS, (iii) MRSA-infected mice treated with unformulated VCM, and (iv) MRSA-infected mice treated with VCM-LIN-P2O NPs. Sepsis was induced through an intraperitoneal (I.P.) injection of 200 μL of MRSA suspension prepared in PBS. One hour post-infection, each group received its respective intraperitoneal treatment: 400 μL of PBS, unformulated VCM (20 mg kg^{-1}), or VCM-LIN-P2O NPs (equivalent to 20 mg kg^{-1} of VCM). Throughout the study, the mice were maintained under controlled environmental conditions (temperature: 19–23 °C; relative humidity: 55 ± 10%) with proper ventilation and were continuously observed for any signs of discomfort or morbidity. After 24 hours, blood samples were collected *via* cardiac puncture to determine bacterial counts (CFU) and to quantify pro-inflammatory cytokine concentrations. Subsequently, the animals were humanely euthanized using isoflurane, and major organs, including the liver, lungs, kidneys, and heart, were excised for bacterial enumeration and histopathological evaluation. In addition, histological analyses were conducted under blinded conditions, but since quantitative measurements were collected directly, blinding was not needed.

2.12.3 Determination of bacterial load. After 24 hours of treatment, blood samples were obtained through cardiac puncture and transferred into heparinized microtubes for the quantification of MRSA CFUs. Subsequently, the organs were carefully excised under aseptic conditions and homogenized in PBS (pH 7.4). The collected blood was diluted at a 1 : 1 ratio, while serial dilutions of the organ homogenates were prepared and plated onto MHA plates. The plates were then incubated at 37 °C for 24 hours, after which the resulting bacterial colonies were counted, and CFU values were calculated using the conventional formula:

$$\text{CFU mL}^{-1} = \frac{\text{Number of colonies} \times \text{Dilution factor}}{\text{Volume plated}}.$$

2.12.4 Quantification of cytokine levels. Plasma levels of sepsis-related cytokines, namely TNF-α, IL-1β, and IL-18, were measured using the LEGENDplex™ multi-analyte flow assay kit (Biocom, South Africa) in accordance with the manufacturer's instructions. Fluorescence acquisition was performed on a DxFLEX flow cytometer (Beckman Coulter, USA). Whole blood samples were centrifuged at 10 000 rpm for 5 minutes, after which the plasma was carefully collected and stored at −80 °C until cytokine analysis.

2.12.5 Histological evaluation. For histopathological analysis, tissue samples from the kidney, lung, liver, and heart of each experimental group were fixed in 4% formaldehyde prepared in PBS. Following fixation, the tissues were embedded in paraffin, sectioned, and stained with hematoxylin and eosin (H&E). The stained sections were then examined under an ApoTome.2 microscope (Carl Zeiss, Germany), and bright-field images were captured using Zen Blue 2.5 Pro software.

2.13 Statistical analysis

Data analysis was carried out using GraphPad Prism® software version 8 (GraphPad Software Inc., USA). Depending on the experimental design, one-way analysis of variance (ANOVA) or unpaired Student's *t*-tests were employed to evaluate statistical significance. All experiments were performed in triplicate, and results are expressed as the mean ± standard deviation (SD). A *p*-value of less than 0.05 was considered indicative of statistical significance. Unless otherwise stated, all graphical representations and illustrations were created using GraphPad Prism 8, FlowJo, and BioRender.

3. Results and discussion

3.1 Molecular docking

During bacterial infections, such as those caused by Gram-positive bacteria, α-H activates ADAM10, whereas PGN and LTH stimulate TLR2 activation.[12,16] The concurrent activation of these receptors disrupts immune homeostasis, resulting in excessive production of pro-inflammatory cytokines, cellular injury, and the progression of sepsis.[45] Therefore, utilizing materials capable of simultaneously targeting ADAM10 and TLR2, thereby preventing the interaction of bacterial toxins

with their respective receptors, represents a promising therapeutic strategy for mitigating bacterial sepsis.

Accordingly, molecular docking analysis was conducted, for the first time, to explore the potential interactions of LIN with ADAM10 and TLR2. As shown in Fig. S1, ADAM10 was docked in the presence of its metal cofactor (Zn) and the substrate α-H. The interaction interface was stabilized through several key hydrogen bonds, including Asp325(A)–Ser159(B), Lys405(A)–Asp4(B), Asp649(A)/Asp651(A)–Asn105(B)/Lys154(B), Gln442(A)–Ser114(B), Arg644(A)/Arg646(A)–Ile98(B)/Pro160(B), and Lys591(A)–Ser99(B)/Asp100(B), with bond lengths ranging from 2.6 to 3.2 Å. Additionally, multiple hydrophobic residues (Leu654, Ala505, Pro606, Leu467, *etc.*) contributed to non-polar stabilization at the binding interface, supporting the formation of a compact and energetically favorable ADAM10-3ANZ complex as predicted by HADDOCK. The top-ranked HADDOCK cluster for ADAM10-3ANZ (HADDOCK score: −117.2 ± 10.7; cluster size: 6; RMSD: 0.6 ± 0.4 Å; *Z*-score: −1.8) exhibited tight convergence, attributed to extensive electrostatic and van der Waals interactions among active site residues.

Subsequent docking of LIN to ADAM10 (Fig. S2) revealed significant hydrophobic interactions, with a binding affinity of −5.8 kcal mol^{-1}, indicating its potential to occupy the same binding pocket as α-H. Furthermore, Fig. 1 depicts the docking results of LTH, PGN, and LIN with TLR2. LIN demonstrated a strong affinity toward TLR2, forming two hydrogen bonds along with several hydrophobic interactions, yielding a binding energy of −7.9 kcal mol^{-1}. In contrast, PGN and LTH exhibited binding affinities of −7.1 kcal mol^{-1} and −6.2 kcal mol^{-1}, respectively.

Overall, these findings suggest that LIN possesses the potential to competitively bind to both ADAM10 and TLR2, thereby inhibiting bacterial toxin binding and attenuating the inflammatory responses associated with bacterial sepsis.

3.2 *In vitro* binding determination of linoleic acid to ADAM10 and TLR2

MST is a highly sensitive biophysical method employed to evaluate the binding affinities between target molecules and

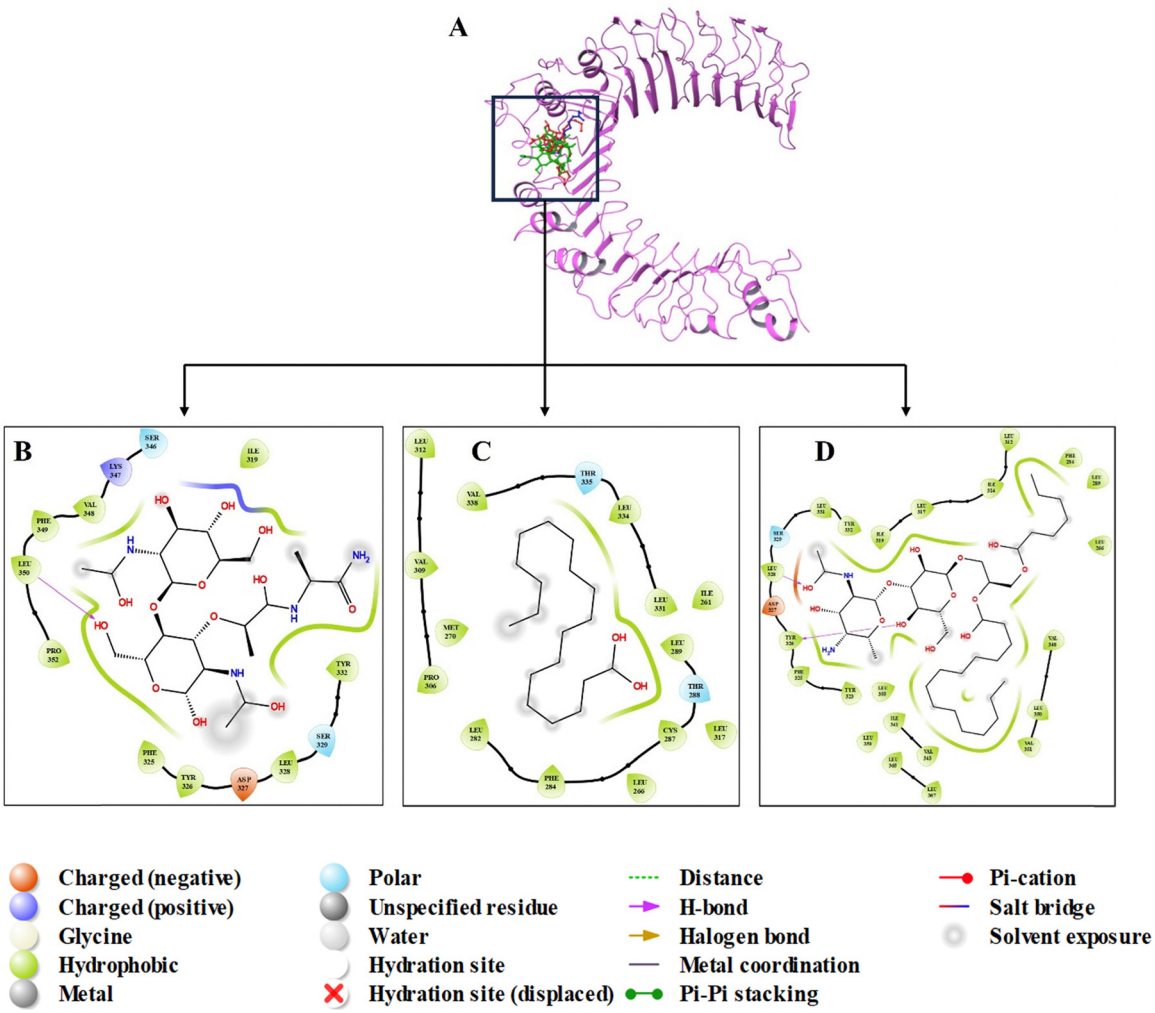

Fig. 1 Docking poses of (A) human TLR2 bound to lipoteichoic acid (LTH) (red), peptidoglycan (PGN) (green), and linoleic acid (LIN) (Blue). (B)–(D) are binding interactions of human TLR2 to lipoteichoic acid, linoleic acid, and peptidoglycan.

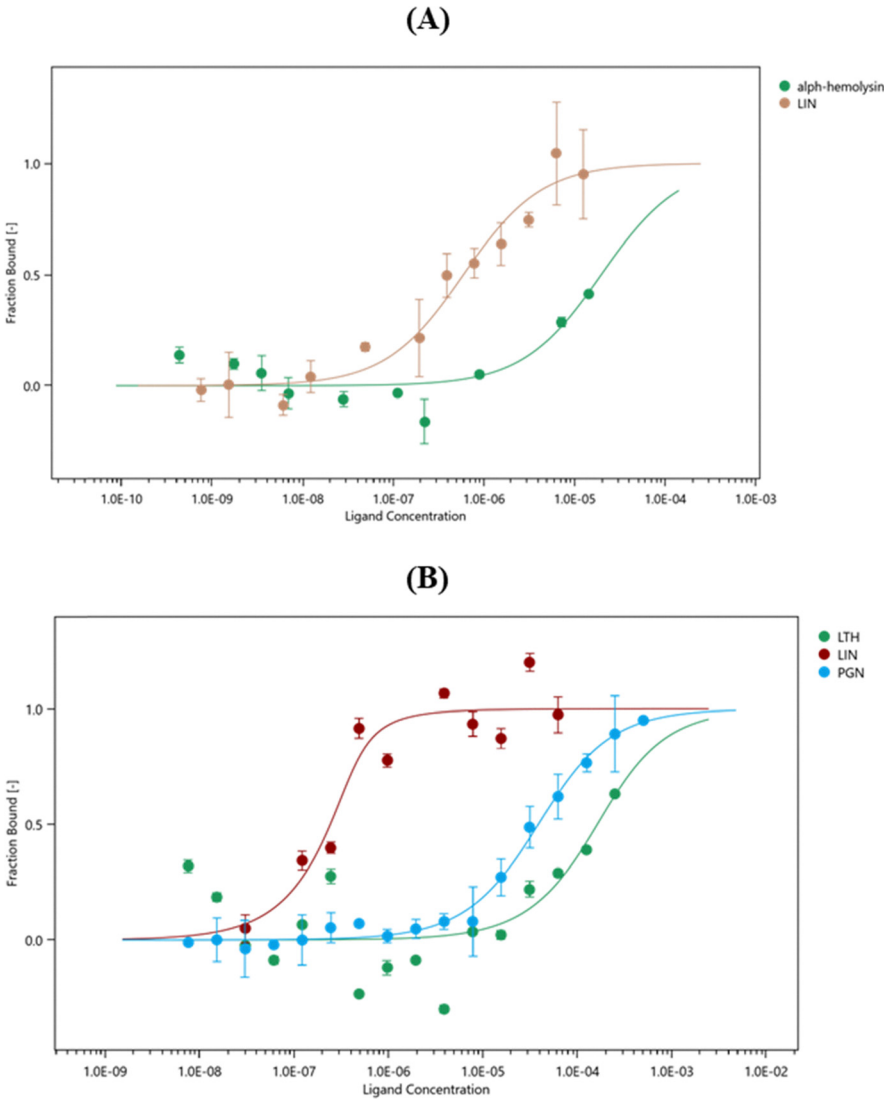

Fig. 2 (A) Comparative binding fractions of linoleic acid (LIN) and alpha-hemolysin (α-H) to ADAM10, showing that LIN exhibited markedly stronger binding affinity than α-H. (B) Comparative binding fractions of LIN, peptidoglycan (PGN), and lipoteichoic acid (LTH) to TLR2, demonstrating that LIN bound with significantly higher affinity relative to PGN and LTH. Data are expressed as mean ± SD (n = 3).

ligands. This technique allows quantitative assessment by detecting variations in thermophoretic movement over different ligand concentrations.[46,47] In this work, MST was applied to validate the molecular docking result of LIN's interactions with ADAM10 compared to α-H, as well as its interactions with TLR2 in relation to PGN and LTH. The binding profiles are illustrated in Fig. 2A, which shows the fraction of ADAM10 bound to LIN and α-H, and Fig. 2B, which depicts the fraction of LIN, PGN, and LTH bound to TLR2. Binding affinities were quantified using the dissociation constant (K_d), where a lower K_d denotes stronger binding, and a higher K_d indicates weaker affinity.[48] As shown in Table 1, LIN demonstrated stronger binding to ADAM10 (K_d = 0.58396 μM) compared to α-H (K_d = 19.692 μM). Similarly, Table 2 reveals that LIN exhibited potent binding to TLR2, with a K_d of 48.02 nM, whereas PGN and LTH displayed significantly weaker affinities, with K_d values of 29.646 μM and 111.74 μM, respectively.

Table 1 The binding affinity (dissociation constant, K_d) of LIN and α-H to ADAM10. All measurements are expressed as mean (n = 3)

Ligand	K_d (μm)
LIN	0.58396
α-H	19.692

Collectively, these findings confirm LIN's favorable binding to ADAM10, which may inhibit ADAM10 activation and the downstream stimulation of NLRP3, while also targeting TLR2 and blocking its signaling cascade. Such dual-targeting activity suggests that LIN may serve as an effective biomimetic adjuvant for antibiotic delivery in bacterial sepsis, potentially improving treatment efficacy.

Table 2 The binding affinity (dissociation constant, K_d) of LIN, PGN, and LTH to TLR2. Measurements are expressed as mean (n = 3)

Ligand	K_d
LIN	48.02 nM
PGN	29.646 μM
LTH	111.74 μM

3.3 Formulation, optimization, and characterization of VCM-LIN-P2O NPs

Leveraging LIN's capacity to bind to ADAM10 and TLR2, HLPNs were developed. The solvent evaporation method was employed to successfully produce both blank LIN-P2O NPs and VCM-LIN-P2O NPs.[22,49] As a preliminary step, different surfactants were screened to identify the most suited for achieving HLPNs with optimal PS, low PDI, and improved stability (Table S1). Based on the stability results, poloxamer 407 (PLX 407) was selected for subsequent experiments.

A one-factor-at-a-time optimization approach was employed to systematically assess various formulation parameters. First, the surfactant-to-lipid ratio was varied (1 : 0.5, 1 : 1, and 1 : 2) while keeping the lipid-to-polymer ratio constant at 1 : 1. Increasing the surfactant proportion led to a progressive increase in particle size from 139.2 nm to 230.5 nm (Table 3). Considering both PS and PDI, the 1 : 1 surfactant-to-lipid ratio was chosen for further optimization.

Next, the effect of the drug-to-system weight ratio was examined at 1 : 2, 1 : 4, 1 : 6, and 1 : 8 ratios (Table 4). Increasing the system weight-to-drug ratio resulted in a corresponding increase in particle size and a rise in EE% up to the 1 : 4 ratio, after which EE% declined. Accordingly, the 1 : 4 ratio was selected for further studies.

Subsequently, the lipid-to-polymer ratio was investigated at 1 : 3, 1 : 1, and 3 : 1 (Table 4). Raising the lipid content from 1 : 1 to 3 : 1 reduced particle size but also lowered EE% (from 53.9% to 42.6%). Conversely, reducing lipid concentration (1 : 3) enhanced EE% to 65.1% but markedly increased the PDI from 0.213 to 0.454. These findings align with previous reports that lipid concentration strongly influences PS and EE% in HLPNs.[25] Based on this evaluation, the 1 : 1 lipid-to-polymer ratio was considered optimal.

Overall, the optimized VCM-LIN-P2O NPs formulation consisted of a surfactant-to-lipid ratio of 1 : 1, a drug-to-system ratio of 1 : 4, and a lipid-to-polymer ratio of 1 : 1. The resulting nanoparticles exhibited a particle size of 141.8 ± 10.113 nm, a PDI of 0.219 ± 0.044, a zeta potential of −19.3 ± 1.48 mV, an EE% of 53.9 ± 2.215%, and a drug loading (DL%) of 10.92 ± 0.250%.

3.4 Surface morphology determination of VCM-LIN-P2O NPs

To further characterize the engineered VCM-LIN-P2O NPs, their surface morphology was examined. As illustrated in Fig. 3, the TEM image revealed uniformly spherical particles with well-defined structure, showing a size distribution that closely correlated with the results obtained from DLS.

3.5 Thermal profile analysis

DSC is a widely employed thermal analysis technique in biomedical nanotechnology, particularly for evaluating drug incorporation within nanocarriers. It provides insight into the physical state of the encapsulated drug by monitoring enthalpic transitions as a function of temperature.[50] The DSC thermograms of P2O, PLX407, trehalose, free VCM, their physical mixture, and lyophilized VCM-LIN-P2O NPs are presented in Fig. S3. Trehalose displayed two characteristic endothermic transitions around 105 °C and 202 °C,[51] while VCM exhibited a sharp endothermic peak around 69 °C followed by a broad decomposition profile.[52] Additionally, PLX407 showed two characteristic endothermic peaks at approximately 71 °C and 393 °C, while P2O demonstrated remarkable thermal stability, remaining stable up to 415 °C.[53] In contrast, the thermogram of VCM-LIN-P2O NPs did not show distinct melting peaks corresponding to VCM or trehalose. The absence of these characteristic transitions suggests that VCM was no longer present in its crystalline form but was instead molecularly dispersed or amorphous within the nanoparticle matrix. On the other hand, the thermogram of the physical mixture retained some of the individual peaks of its constituents, indicating the lack of significant intermolecular interactions in the absence of nanoparticle formation.

This thermal behavior collectively confirms successful encapsulation of VCM within the nanosystem, with molecular dispersion contributing to the stability and potential bioavailability advantages of the formulation.

3.6 *In vitro* biocompatibility studies

3.6.1 *In vitro* cytocompatibility. Biosafety and biocompatibility are fundamental prerequisites for the clinical translation of any novel compound in biomedical and pharmaceutical applications.[54] In this study, the cytocompatibility of VCM-LIN-P2O NPs was assessed using the MTT cell viability assay in HEK-293, HepG2, and RAW264.7 cell lines (Fig. 4A). The

Table 3 Size, PDI, and ZP for different surfactant-to-lipid weight ratios used in the optimization of VCM-LIN-P2O NPs. Results represented as mean ± SD (n = 3)

Optimization parameter	Size (nm)	PDI	ZP (mV)
Surfactant-to-lipid ratio	Fixed lipid polymer ratios (1 : 1) with total system 70 mg		
1 : 0.5	139.2 ± 2.516	0.340 ± 0.007	−24.3 ± 5.32
1 : 1	141.18 ± 10.81	0.213 ± 0.007	−19.8 ± 0.400
1 : 2	230.5 ± 2.987	0.465 ± 0.034	−27.3 ± 5.85

Table 4 Size, PDI, ZP, EE%, and DL% for different lipid: polymer mass ratios and sonication times used in the optimization of VCM-LIN-P2O NPs. Results represented as mean ± SD (n = 3)

Optimization parameter	Size (nm)	PDI	ZP (mV)	EE%	DL% w/w
Drug-to-system weight ratio	Fixed VCM weight (10 mg)				
1 : 2	133.1 ± 1.051	0.189 ± 0.008	−20.6 ± 0.557	49.25%	9.84%
1 : 4	141.18 ± 10.81	0.213 ± 0.007	−19.8 ± 0.400	53.95%	7.71%
1 : 6	155.5 ± 0.1528	0.194 ± 0.006	−18.6 ± 1.68	50.611%	5.62%
1 : 8	179.4 ± 3.075	0.221 ± 0.021	−17.7 ± 0.874	44.07%	4.01%
Lipid-to-polymer mass ratio	Fixed system weight (70 mg), with VCM 10 mg and surfactant 20 mg				
1 : 3	144.1 ± 0.3786	0.159 ± 0.036	−16.7 ± 1.14	42.6%	6.09%
1 : 1	141.18 ± 10.81	0.213 ± 0.007	−19.8 ± 0.400	53.95%	7.71%
3 : 1	89.97 ± 0.0723	0.454 ± 0.010	−18.6 ± 0.569	65.151%	9.31%

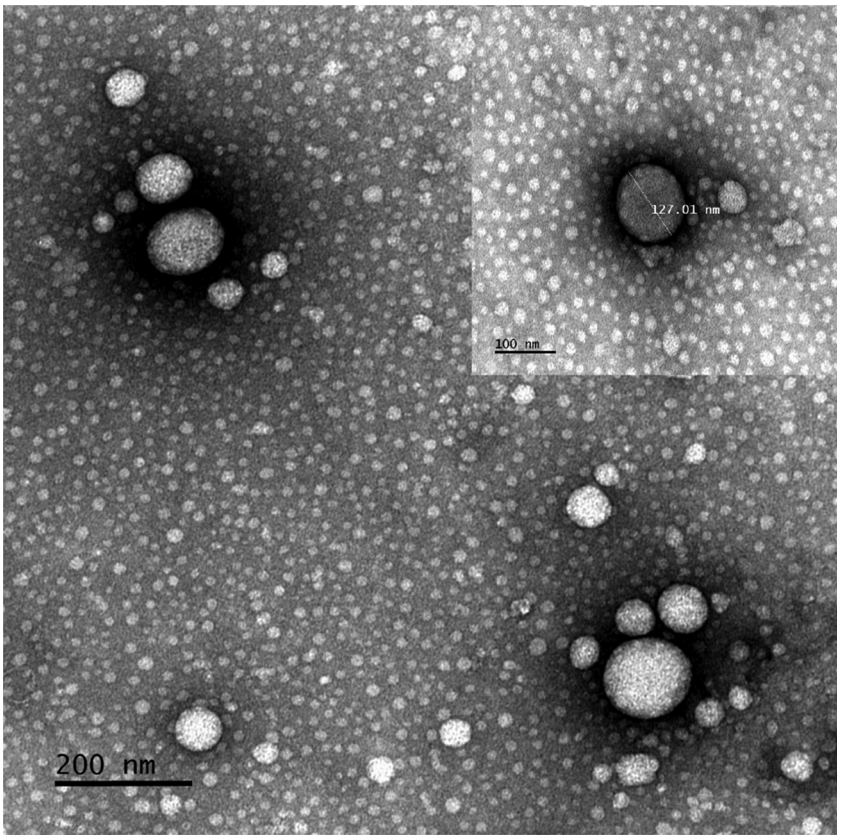

Fig. 3 TEM image of VCM-LIN-P2O NPs.

nanoparticles maintained cell viability above 75% across all tested concentrations, with no clear dose-dependent cytotoxicity observed except in HEK-293 cells. Even in this case, cell viability remained above 90% at the highest concentration. Specifically, VCM-LIN-P2O NPs exhibited viability values ranging from 91.4% to 98.6% in HEK 293 cells, 83.4% to 75.02% in HepG2 cells, and 119.3% to 92.8% in RAW264.7 cells. Interestingly, in the RAW264.7 cell line, the nanoparticles appeared to support normal cellular function and progression, indicating not only survival but also maintenance of metabolic activity. According to the International Organization for Standardization (ISO) guidelines on biomedical product biocompatibility, materials are considered non-cytotoxic if they retain $\geq$70% cell viability.[55] Based on these criteria, VCM-LIN-P2O NPs can be classified as non-toxic, supporting their safety and potential as promising NDS for biomedical applications.

3.6.2 *In vitro* hemocompatibility. Hemocompatibility is a crucial factor in evaluating the biosafety of nanomedicines intended for intravenous administration.[56,57] To assess this, the effect of the synthesized VCM-LIN-P2O NPs on erythrocytes was examined using freshly collected and washed sheep blood, with the results shown in Fig. 4B. The nanoparticles induced

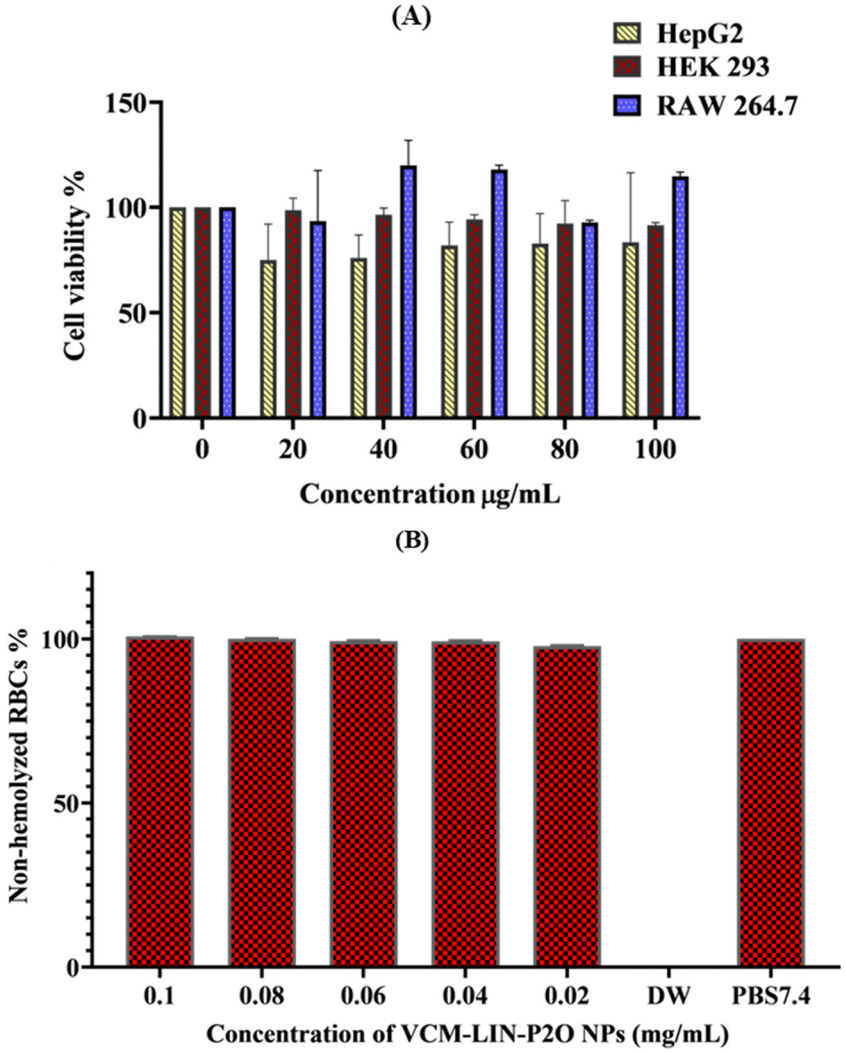

Fig. 4 (A) Cell viability percentages of HEK-293, HepG2, and RAW264.7 cell lines following exposure to different concentrations of VCM-LIN-P2O NPs compared with controls. (B) Hemolytic activity of VCM-LIN-P2O NPs at various concentrations (DW = distilled water; PBS = phosphate-buffered saline, pH 7.4). All values in the graphs are presented as mean ± SD (n = 3).

less than 3% hemolysis at all tested concentrations, confirming their non-hemolytic nature and favorable safety profile. These findings are consistent with the previously demonstrated cytocompatibility of VCM-LIN-P2O NPs, further supporting their suitability for safe intravenous application.

3.7 *In vitro* drug release and kinetics

The release kinetics of VCM from VCM-LIN-P2O NPs were investigated *in vitro* over 48 hours using the dialysis bag diffusion method, with bare VCM included as a control. The cumulative release of bare VCM at 1, 6, 12, and 24 hours was 20.1%, 70.06%, 95.2%, and 100%, respectively. In contrast, VCM-LIN-P2O NPs exhibited cumulative release values of 17.24%, 44.68%, 61.67%, and 81.4% at the same time points (Fig. 5). These data demonstrate a statistically significant difference in release rates between the bare VCM and the nanoformulation. Overall, bare VCM exhibited a rapid release profile, achieving complete drug diffusion across the dialysis membrane within 24 hours. Conversely, the nanoformulation displayed a sustained release pattern, attributed to the gradual diffusion of drug molecules through the lipid–polymer matrix, which prolongs VCM retention.[58] This sustained release behavior is consistent with previously reported findings, which showed that approximately 50% of VCM entrapped within HLPNs was released within 24 hours.[19,58]

To further characterize the release mechanism of VCM from VCM-LIN-P2O NPs under physiological conditions, the cumulative release data were fitted to various kinetic models using the DDSolver software[40] (Table S2). The release profile was best described by the Weibull model, as indicated by the highest correlation coefficient (R^2 = 0.9990) and the lowest root mean square error (RMSE = 0.7770). The calculated Weibull exponent parameter (β) was 0.814, reflecting the mechanism of drug transport through the nanoparticle matrix. According to Papadopoulou *et al.* (2006), a β value between 0.75 and 1.0 indicates that drug release is governed by a combination

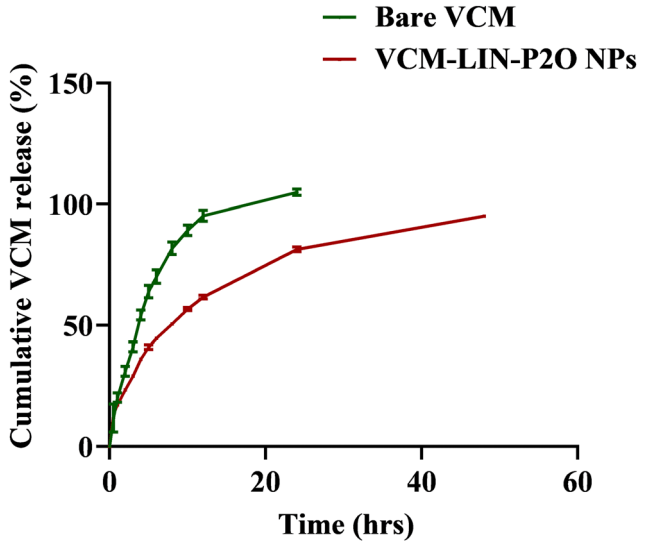

Fig. 5 Comparative releases of VCM from VCM-LIN-P2O NPs and bare VCM under physiological pH (7.4). data are expressed as mean ± SD (n = 3).

of Fickian diffusion and case II transport, whereas a β value below 0.75 suggests predominantly Fickian diffusion.[59] Based on this criterion, the release of VCM from VCM-LIN-P2O NPs can be attributed to a mixed mechanism involving both Fickian diffusion and case II transport.

3.8 Physical stability of VCM-LIN-P2O NPs

The physical stability of VCM-LIN-P2O NPs was assessed over a three-month period under two storage conditions: refrigerated condition (4 °C) and room temperature (RT). This evaluation aimed to investigate the influence of storage temperature and duration on critical physicochemical attributes, including PS, PDI, and ZP, as well as macroscopic indicators of stability, such as aggregation and sedimentation (Table 5). Under both storage conditions, the formulation maintained excellent physical stability throughout the study, as indicated by the absence of visible signs of instability and statistically insignificant variations in PS, PDI, and ZP (p-value $>$ 0.05). These results demonstrate that VCM-LIN-P2O NPs remain physically stable under both refrigerated and normal (RT) conditions for up to three months. Future investigations should include chemical stability studies of VCM within the formulation to provide comprehensive stability data and inform further optimization.

3.9 *In vitro* antibacterial activity

3.9.1 Determination of MIC. The MICs of bare VCM, blank LIN-P2O NPs, and VCM-LIN-P2O NPs were determined by the microdilution assay against both methicillin-sensitive and methicillin-resistant SA (SA and MRSA). As summarized in Table 6, the MIC of bare VCM and VCM-LIN-P2O NPs against SA remained comparable, with values of 1.95 μg mL^{-1} maintained up to 72 hours. These results indicate that the nanoformulation successfully retained the intrinsic antibacterial activity of VCM while offering the additional advantages of prolonged systemic circulation and the potential to mitigate dose-related adverse effects. Against MRSA, both bare VCM and VCM-LIN-P2O NPs initially exhibited similar MICs (7.812 μg mL^{-1}) at 24 hours. However, by 48 hours, bare VCM showed a loss of antibacterial activity, as evidenced by an MIC increase from 7.812 μg mL^{-1} to 15.63 μg mL^{-1}. In contrast, the MIC of VCM-LIN-P2O NPs remained unchanged over 48 and 72 hours, representing a two-fold enhancement in efficacy relative to bare VCM. The superior and sustained antibacterial activity of VCM-LIN-P2O NPs against MRSA is likely attributable to the sustained release of VCM, in addition to the presence of P2O, which has been reported to possess inherent anti-MRSA properties.[29] These findings are consistent with previous reports demonstrating sustained MIC values for VCM-loaded HLPNs and polymeric nanocarriers against both SA and MRSA.[11,60]

3.9.2 MRSA-killing kinetics. To evaluate the bactericidal activity of bare VCM and VCM-LIN-P2O NPs against MRSA, an *in vitro* time-kill assay was conducted. As shown in Fig. 6A, the bacterial killing kinetics revealed that VCM-LIN-P2O NPs exhibited markedly superior efficacy, achieving complete (100%) eradication of MRSA within 24 hours. In contrast, bare VCM failed to fully eliminate the bacterial population even after 24 hours of incubation, underscoring the significantly enhanced antibacterial activity of the nanoparticle formulation. These findings are consistent with previously reported NDS for VCM

Table 6 *In vitro* antibacterial activity of bare VCM, VCM-LIN-P2O NPs, and blank LIN-P2O NPs, expressed as MIC values (μg mL^{-1}) against Gram-positive bacteria (MRSA and SA) at pH 7.4. All measurements are shown as mean ± SD (n = 3)

	SA (MIC μg mL^{-1})			MRSA (MIC μg mL^{-1})		
	24	48	72	24	48	72
VCM	1.95	1.95	1.95	7.8125	15.625	15.625
VCM-LIN-P2O NPs	1.95	1.95	1.95	7.8125	7.8125	7.8125
BLANK-LIN-P2O NPs	NA	NA	NA	NA	NA	NA

Table 5 Effect of storage conditions and duration on the physical stability of VCM-LIN-P2O NPs. Data are presented as mean ± SD (n =3)

Storage condition	Ambient temperature (25 °C)			4 °C		
Time (days)	PS (nm)	PDI	ZP (mV)	PS (nm)	PDI	ZP (mV)
0	118.3 ± 0.08185	0.257 ± 0.007	−13.5 ± 1.61	118.3 ± 1.08185	0.257 ± 0.007	−13.5 ± 1.61
30	118.4 ± 0.8183	0.266 ± 0.009	−11.3 ± 0.985	115.2 ± 1.6028	0.274 ± 0.008	−11.9 ± 2.11
60	120.8 ± 2.08	0.266 ± 0.008	−8.35 ± 1.36	114.4 ± 2.55	0.289 ± 0.004	−11.5 ± 0.586
90	120.7 ± 2.004	0.277 ± 0.003	−9.6 ± 1.03	114.0 ± 2.6506	0.270 ± 0.0917	−12.5 ± 1.17

delivery, which demonstrated notable improvements in bacterial clearance rates. For instance, Osman *et al.* (2024) reported total eradication within 8 hours at pH 6, although eradication was not achieved at pH 7.4,[61] whereas Nwabuife *et al.* (2023) observed complete clearance within 12 hours.[62] Collectively, these results highlight the potential of VCM-LIN-P2O NPs as a promising strategy for the effective treatment of MRSA infections and the prevention of severe outcomes such as sepsis. The enhanced antibacterial efficacy may enable dose reduction and shorter treatment durations, ultimately improving therapeutic outcomes and minimizing the risk of resistance development.

3.9.3 MRSA membrane disruption. P2O has been reported to possess inherent antibacterial activity by mimicking host defense peptides, leading to membrane lysis in MRSA.[29] This membrane-disruption property is particularly advantageous, as it lowers the likelihood of bacteria developing resistance. Building on this characteristic, the ability of VCM-LIN-P2O NPs to disrupt MRSA cell membranes was examined using TEM. MRSA cultures were incubated for 4 hours with either bare VCM or VCM-LIN-P2O NPs at concentrations corresponding to five times their MIC values, while PBS (pH 7.4) served as the negative control. Fig. 6B compares the structural morphology of bacterial membranes across the different treatment groups. Both the PBS-treated control and bare VCM-treated groups displayed intact bacterial envelopes with smooth surfaces and uniformly distributed cytoplasm. In contrast, MRSA exposed to VCM-LIN-P2O NPs exhibited severe membrane damage, including surface disruption, loss of structural integrity, and marked cytoplasmic disorganization.

Taking all together, these findings demonstrate that VCM-LIN-P2O NPs exert a stronger membrane-disruptive effect than bare VCM, underscoring their potential as a more potent antibacterial strategy for combating MRSA infections.

3.10 *In vitro* antioxidant activity

3.10.1 DPPH scavenging assay. Sepsis microenvironment is characterized by excessive production of reactive oxygen species (ROS) as a consequence of a dysregulated immune response to infection. This overproduction of ROS contributes to cellular injury, organ dysfunction, and increased mortality.[63] Addressing this challenge, the development of NDS with ROS-scavenging capability could help mitigate inflammation, improve sepsis management, and reduce associated complications.

The antioxidant potential of VCM-LIN-P2O NPs and their individual components (LIN and P2O) was assessed using a DPPH radical scavenging assay, with ascorbic acid (AS) serving as the positive control. Fig. 7A shows the percentage of DPPH radical scavenging for AS, LIN, P2O, and VCM-LIN-P2O NPs following incubation at 37 °C in the dark. The scavenging activities were quantified as 28.99 ± 4.30% for P2O, 30.80 ± 4.06% for LIN, and 35.88 ± 3.60% for VCM-LIN-P2O NPs. Although P2O exhibited moderate scavenging activity, it's likely a result of nonspecific physical interactions with DPPH radicals

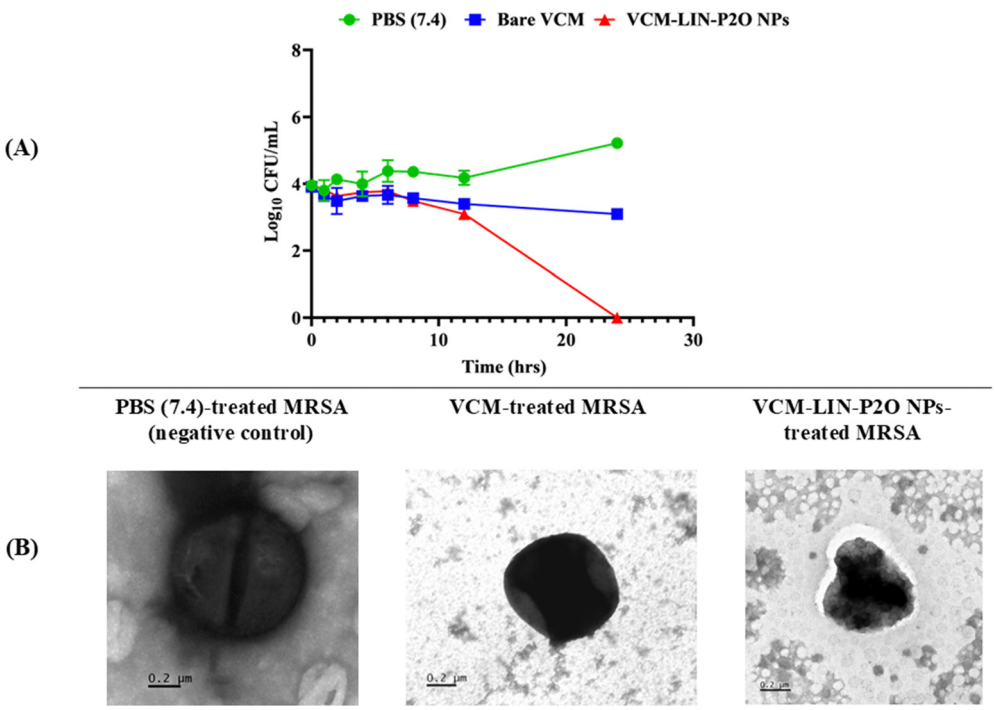

Fig. 6 (A) Time-kill kinetics of MRSA following exposure to 5 × MIC of bare VCM, VCM-LIN-P2O NPs, or PBS (pH 7.4) as a negative control, demonstrating the superior bactericidal activity of the nanoparticle formulation. All values are presented as mean ± SD (n = 3). (B) TEM image of MRSA cells: PBS-treated and bare VCM-treated groups display intact cell membranes with preserved morphology, whereas VCM-LIN-P2O NPs treatment results in extensive membrane disruption, loss of structural integrity, and cytoplasmic disorganization.

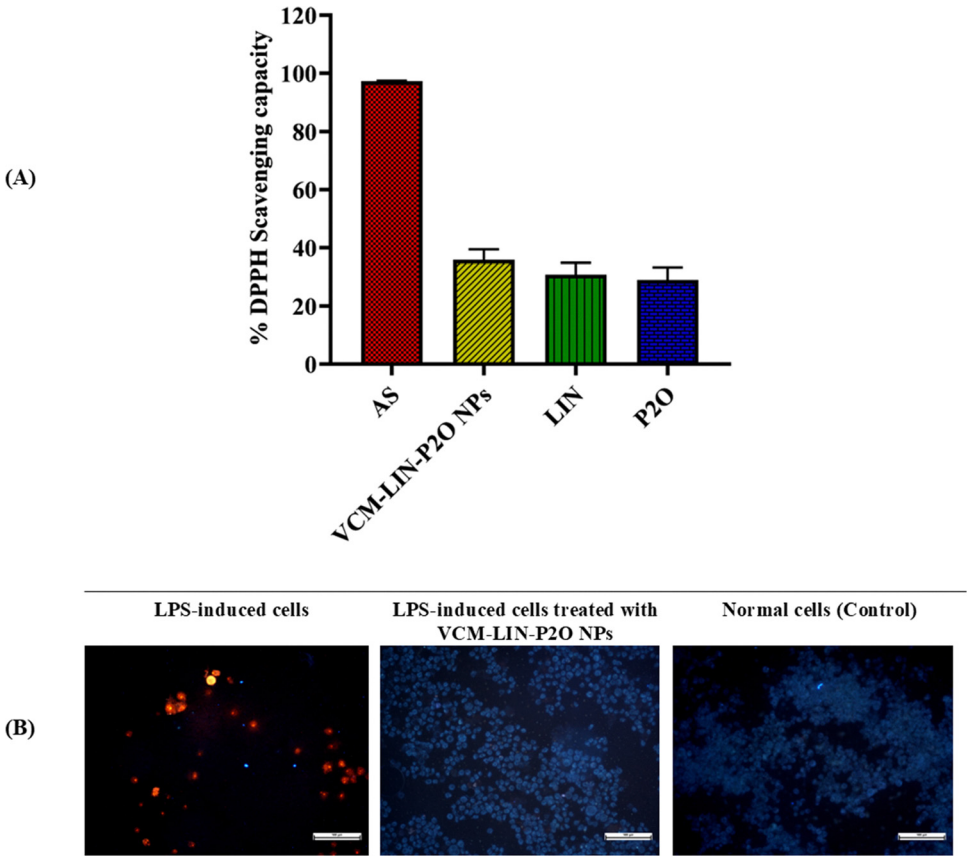

Fig. 7 *In vitro* antioxidant activity. (A) The ability of VCM-LIN-P2O NPs to neutralize DPPH radicals, compared with their individual components (P2O, LIN) and ascorbic acid (AS), which served as the positive control. All values are shown as mean ± SD (n = 3). (B) Visualization of mitochondrial ROS levels in RAW 264.7 cells using MitoSOX™ Red under a fluorescence microscope. Treatment with VCM-LIN-P2O NPs after LPS stimulation led to a clear drop in red fluorescence intensity, bringing ROS levels close to those seen in the untreated control group.

rather than direct chemical neutralization. In contrast, the significantly higher scavenging observed for VCM-LIN-P2O NPs can be primarily attributed to LIN, whose potent antioxidant and anti-inflammatory properties have been well-documented.[26]

3.10.2 ROS scavenging at the mitochondrial level. Previous studies have demonstrated that scavenging excessive ROS can alleviate the severity of sepsis and improve disease management.[63,64] To further investigate the antioxidant potential of VCM-LIN-P2O NPs, RAW 264.7 cells were pre-treated with LPS, 1 μg mL^{-1}, for 4 hours to induce intracellular ROS production and an inflammatory response. Following this induction phase, the cells were exposed to VCM-LIN-P2O NPs and incubated for an additional 14 hours.

Mitochondrial ROS levels were assessed using the MitoSOX™ Red probe, and fluorescence was visualized under a fluorescence microscope. As shown in Fig. 7B, LPS-stimulated cells exhibited intense red fluorescence, confirming elevated mitochondrial ROS production. In contrast, cells treated with VCM-LIN-P2O NPs displayed fluorescence levels comparable to those of untreated controls, indicating effective ROS scavenging. Moreover, the observed ROS-reducing effect of VCM-LIN-P2O NPs aligns with previous reports on nanocarriers designed to target intracellular ROS in other oxidative stress-related conditions, such as diabetic foot injury.[64]

Based on the above, these results confirm the robust ROS-scavenging activity of VCM-LIN-P2O NPs, in agreement with the DPPH assay findings, and highlight their potential to attenuate oxidative stress and improve therapeutic outcomes in sepsis management.

3.11 *In vitro* anti-inflammatory activity

Sepsis is characterized by a vast release of pro-inflammatory cytokines, which play a central role in driving tissue injury and accelerating the progression to multi-organ failure.[63] Consequently, quantifying these cytokines is a critical step in assessing the ability of NDS to mitigate sepsis-associated inflammation. Among the major mediators involved, IL-1β and TNF-α are well-established contributors to sepsis pathophysiology.[65] In this study, we examined the capacity of VCM-LIN-P2O NPs to inhibit the secretion of IL-1β and TNF-α in RAW264.7 cell line challenged with bacterial LPS, comparing their performance to that of bare VCM. This evaluation aimed to determine whether the nanoformulation could more effectively attenuate the excessive inflammatory response characteristic of sepsis. Exposure of RAW 264.7 cells to LPS (1 μg mL^{-1}) triggered a robust increase in IL-1β and TNF-α levels (p-value < 0.0001), as shown in Fig. 8. Treatment with VCM-LIN-P2O NPs significantly suppressed the production of both IL-1β (p-value < 0.0001) and TNF-α

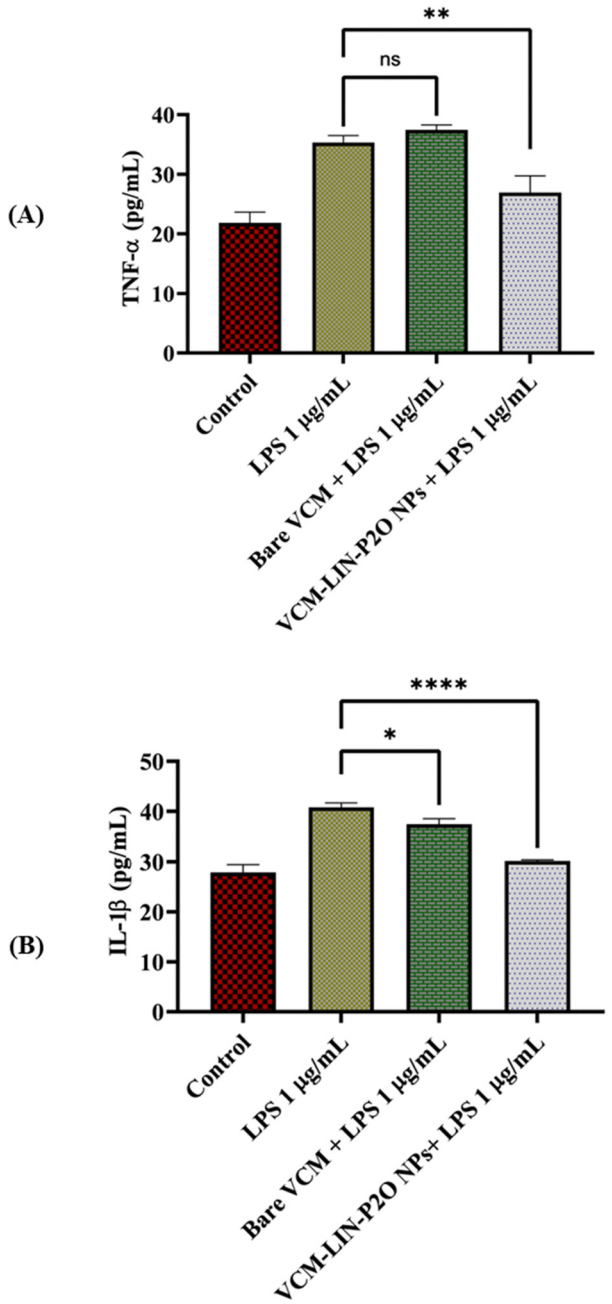

Fig. 8 Effect of VCM-LIN-P2O NPs and bare VCM on (A) TNF-α and (B) IL-1β secretion in LPS-stimulated RAW 264.7 cells. Treatment with VCM-LIN-P2O NPs significantly reduced the secretion of both IL-1β and TNF-α, whereas bare VCM produced a significant decrease only in IL-1β levels and showed no measurable effect on TNF-α. Data are presented as mean ± SD (n = 3). Statistical significance is indicated as ****p-value < 0.0001, **p-value < 0.01, and *p-value < 0.05.

(p-value = 0.00130). By contrast, bare VCM elicited only a moderate but statistically significant reduction in IL-1β levels (p = 0.0114) and had no significant effect on TNF-α secretion. The pronounced anti-inflammatory activity observed with VCM-LIN-P2O NPs may stem from their strong and competitive interactions with ADAM10 and TLR2 receptors, as supported by both computational and experimental evidence in this work.

Overall, these findings highlight VCM-LIN-P2O NPs as a promising therapeutic strategy for regulating pro-inflammatory cytokine release and mitigating the dysregulated immune response associated with sepsis.

3.12 *In vivo* antisepsis potential of VCM-LIN-P2O NPs in MRSA-induced sepsis in a mice model

To translate the promising *in vitro* outcomes into a preclinical setting, an *in vivo* study was performed using a BALB/c mice model of MRSA-induced sepsis. As depicted in Fig. 9A, mice were infected with MRSA and, one hour later, received intraperitoneal injections (I.P.) of either PBS, bare VCM (20 mg kg^{-1}), or VCM-LIN-P2O NPs containing an equivalent VCM dose (20 mg kg^{-1}). After 24 hours, blood was collected *via* cardiac puncture. Whole blood samples were used to determine bacterial burden, while plasma, separated by centrifugation, was analyzed for inflammatory cytokine concentrations. Subsequently, the animals were humanely euthanized, and vital organs (kidneys, lungs, liver, and heart) were collected for bacterial load determination and histopathological evaluation.

3.12.1 Determination of bacterial load. Given the strong link between bacterial burden and sepsis severity, treatment efficacy was evaluated by quantifying MRSA CFUs in the bloodstream, kidney, heart, liver, and lung.[42,66] As shown in Fig. 9B, administration of bare VCM did not produce a statistically significant reduction in blood bacterial load (p-value = 0.4366). In contrast, treatment with VCM-LIN-P2O NPs resulted in a highly significant decrease in CFUs (p-value < 0.0001), representing a 90.97% reduction in circulating bacteria.

Similarly, organ-specific bacterial loads were assessed in the heart, kidneys, liver, and lungs (Fig. 9C–F). bare VCM led to a significant bacterial reduction only in the kidneys (p-value = 0.0052), with no meaningful effect observed in the other organs. Conversely, VCM-LIN-P2O NPs achieved significant bacterial clearance in all organs tested, with p-value < 0.0001 for the heart and kidneys, and p-value = 0.0451 and p-value = 0.0187 for the lungs and liver, respectively. These results clearly demonstrate that a single dose of VCM-LIN-P2O NPs provides superior antibacterial efficacy across multiple tissues, including blood, kidney, lung, liver, and heart, when compared to bare VCM. The enhanced therapeutic outcome is consistent with the *in vitro* antibacterial findings of this study and may be attributed to the targeted delivery of VCM to infection sites and the intrinsic antibacterial activity of P2O.[29]

3.12.2 Determination of inflammatory marker levels. During sepsis, the uncontrolled release of pro-inflammatory cytokines is a key driver of tissue injury and the cascade leading to multi-organ failure.[67] Given the previously demonstrated ability of LIN to interact with ADAM10, thereby inhibiting NLRP3 inflammasome activation, and to bind TLR2, collectively reducing the cytokine storm characteristic of sepsis, its anti-inflammatory potential was further examined *in vivo*. To this end, plasma levels of IL-1β and IL-18, two primary markers of NLRP3 inflammasome activation,[21,67] along with TNF-α, a major inflammatory cytokine implicated in sepsis,[42] were measured to evaluate the therapeutic efficacy of VCM-LIN-P2O NPs.

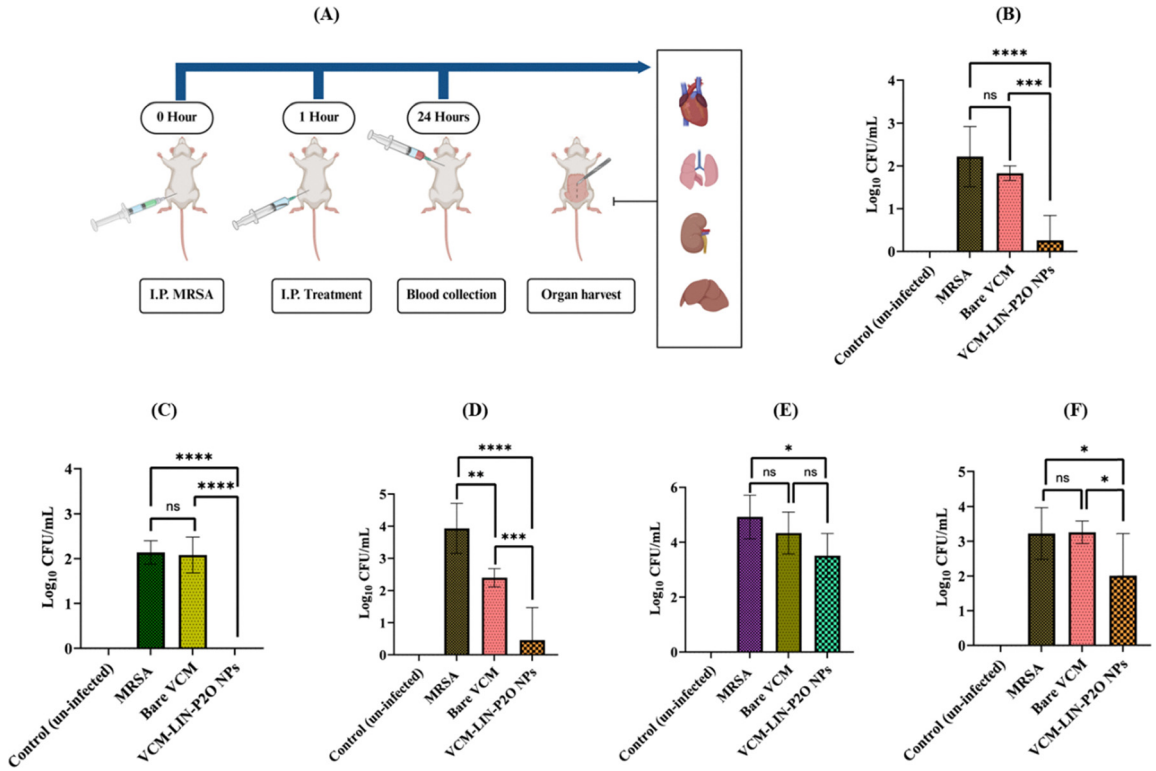

Fig. 9 *In vivo* evaluation of the therapeutic efficacy of VCM-LIN-P2O NPs compared with bare VCM in a BALB/c mice model of MRSA-induced sepsis. (A) Experimental design: sepsis was induced by intraperitoneal (I.P.) MRSA challenge, followed by I.P. administration of treatments 1 h post-infection. After 24 h, blood and major organs (heart, lungs, liver, and kidneys) were collected for further analysis. (B) Bacterial burden in blood, showing 90.97% clearance with VCM-LIN-P2O NPs. (C)–(F) Bacterial loads in the heart, kidneys, liver, and lungs, respectively. VCM-LIN-P2O NPs eliminated bacteria from the heart and significantly reduced bacterial counts in all other organs. Data are expressed as mean ± SD (n = 6); *p < 0.05, **p < 0.01, ***p < 0.001, ****p < 0.0001.

The study compared the effects of bare VCM and VCM-LIN-P2O NPs on the modulation of these cytokines in an MRSA-induced sepsis model.

As depicted in Fig. 10A–C, treatment with VCM-LIN-P2O NPs significantly reduced all three cytokines compared to infected but untreated mice, whereas bare VCM failed to produce a statistically significant decrease. Specifically, VCM-LIN-P2O NPs administration resulted in a 12.8-fold (p-value = 0.0091), 3.4-fold (p-value = 0.0377), and 4.14-fold (p-value < 0.0001) reduction in TNF-α, IL-1β, and IL-18 levels, respectively,

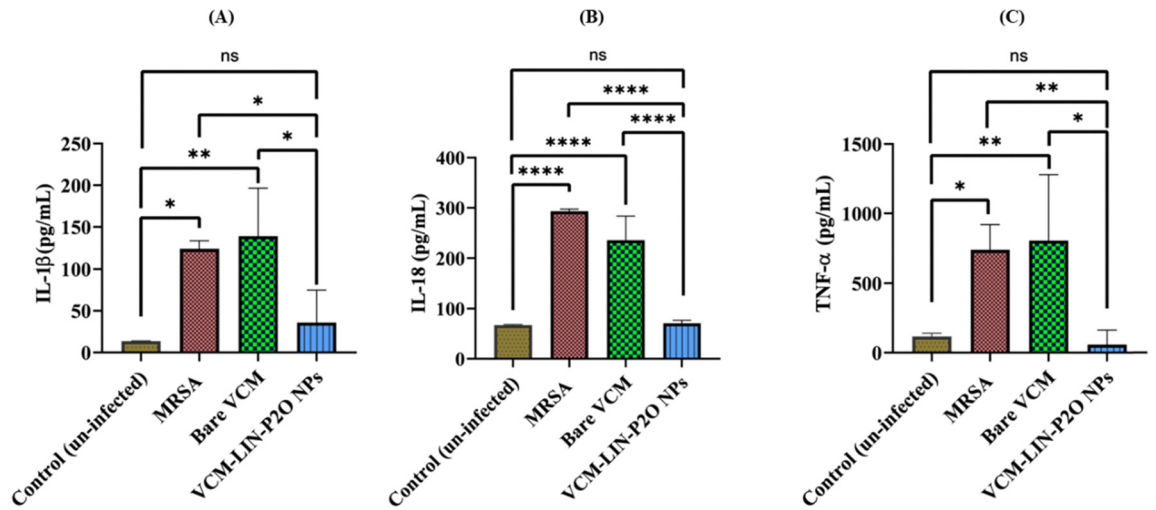

Fig. 10 Effects of various treatments on plasma levels of sepsis-associated pro-inflammatory cytokines: (A) IL-1β, (B) IL-18, and (C) TNF-α. Treatment with VCM-LIN-P2O NPs significantly decreased the concentrations of IL-1β, IL-18, and TNF-α. Data are expressed as mean ± SD (n = 6).

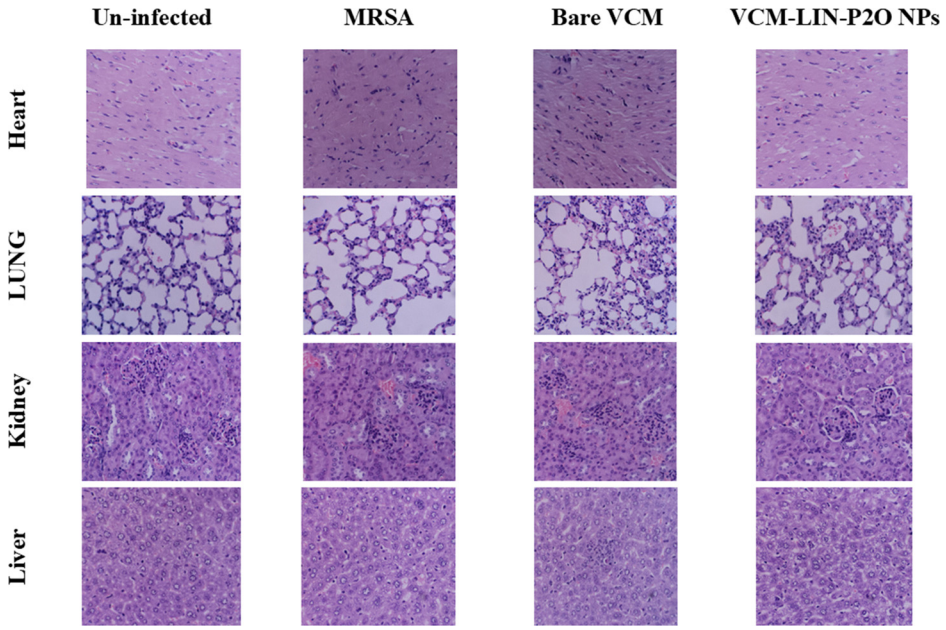

Fig. 11 Histological examination of heart, lung, kidney, and liver sections from MRSA-infected BALB/c mice (H&E staining, original magnification ×20) following treatment with PBS, free vancomycin (VCM), or VCM-LIN-P2O NPs.

compared to bare VCM, which didn't show any significant reduction. This pronounced downregulation of pro-inflammatory mediators is likely driven by the LIN component within VCM-LIN-P2O NPs, which demonstrated strong interactions with ADAM10 and TLR2 in both computational and *in vitro* assays, thereby exerting potent anti-inflammatory effects in the context of bacterial sepsis.

3.12.3 Histological assessment. Sepsis induced by MRSA is associated with severe multiorgan injury, which leads to organ failure and death.[68] To evaluate histopathological changes associated with sepsis, mice were sacrificed 24 hours post-infection, and tissues were examined by H&E staining under a light microscope.

MRSA-infected livers exhibited edema, necrosis, and disorganized hepatic plates, which were only slightly improved by bare VCM but substantially restored by VCM-LIN-P2O NPs (Fig. 11). Similarly, kidneys from infected mice showed Bowman's space disruption and debris accumulation, with minimal improvement by bare VCM, whereas VCM-LIN-P2O NPs markedly preserved renal structure. Moreover, cardiac tissue from infected mice displayed degeneration and hemorrhage, both of which were alleviated by treatment, with greater improvement observed in the nanoformulation group. Furthermore, the lungs of infected mice revealed congestion, necrosis, and neutrophil infiltration, partially reduced by bare VCM but significantly improved with VCM-LIN-P2O NPs.

Taking all together, these findings indicate that VCM-LIN-P2O NPs confer superior protection against MRSA-induced histopathological damage compared to bare VCM, preserving organ architecture and reducing the risk of sepsis-associated organ failure.

4. Conclusion

The design and application of biomimetic materials that can selectively target more than one inflammatory pathway offer a promising avenue for developing next-generation antibiotic NDS to treat bacterial sepsis. Such advanced systems not only enable targeted drug delivery but also help regulate dysregulated immune responses, thereby improving overall sepsis management and reducing complications. In this study, a novel dual-targeting biomimetic HLPNs was developed by integrating LIN with P2O to achieve targeted delivery of VCM against bacterial sepsis. The anti-inflammatory activity of LIN was investigated through its ability to interact with ADAM10, inhibiting NLRP3 inflammasome activation, and simultaneously modulating TLR2 signaling, ultimately attenuating the cytokine storm characteristic of sepsis. A computational approach study confirmed that LIN binds with high affinity to human ADAM10 and TLR2 compared with their natural ligands, and these results were further supported by *in vitro* MST analysis. Moreover, the resulting VCM-LIN-P2O NPs exhibited excellent physicochemical characteristics, high biocompatibility, a sustained VCM release profile, and potent antibacterial activity against both methicillin-susceptible and methicillin-resistant SA. In addition, they demonstrated strong free-radical scavenging ability and anti-inflammatory properties *in vitro*. *In vivo* evaluation using a murine sepsis model revealed that VCM-LIN-P2O NPs significantly lowered bacterial loads in the blood and peripheral organs, including the liver, kidney, heart, and lung, reduced pro-inflammatory cytokine levels, and alleviated organ injury. Importantly, these outcomes surpassed those achieved with untreated controls and bare VCM treatment.

Although these findings are highly encouraging, further optimization is needed to improve scalability, reproducibility, and the long-term chemical and biological stability of the formulation. In addition, extensive cellular studies to support mechanistic investigations, including direct assessment of ADAM10 signaling and TLR2, as well as antioxidant activity, are needed to substantiate the proposed modes of action. Moreover, comprehensive biosafety evaluations, including pharmacokinetic, immunogenicity, and toxicity assessments in relevant preclinical and clinical models, will be critical before advancing toward clinical application.

Finally, our results highlight the dual-targeting potential of LIN, a natural compound with an excellent safety profile, as a promising component of NDS capable of enhancing antibiotic delivery while modulating immune responses in bacterial sepsis. This work lays the groundwork for the rational design of biomimetic platforms that could reshape the therapeutic approach to sepsis.

Author contributions

Abdelrahman Tageldin: conceptualization, data curation, formal analysis, investigation, methodology, validation, visualization, writing – original draft, writing – review & editing. Calvin A. Omolo: conceptualization, supervision, investigation, methodology, validation, writing – review & editing. Vincent O. Nyandoro: conceptualization, methodology, investigation. Mohammed A. Gafar: methodology, investigation, writing – review & editing. Eman A. Ismail: methodology, investigation. Lucy W. Kiruri: methodology, investigation. Bongani B. Nkambule: methodology, investigation. Irene Makraj: methodology, investigation. Thirumala Govender: conceptualization, funding acquisition, supervision, validation, writing – review & editing.

Conflicts of interest

The authors declare no relevant financial or non-financial interests.

Data availability

The data supporting the findings of this study are available within the article and its supplementary information (SI). Supplementary information is available. See DOI: https://doi.org/10.1039/d6tb00207b.

Acknowledgements

This work was supported by the National Research Foundation, South Africa (NRF Grant No. CPRR23032086645) and the College of Health Sciences, University of KwaZulu-Natal. The authors are grateful to the College of Health Sciences and the Biomedical Resource Unit at the University of KwaZulu-Natal (UKZN), as well as the UKZN Novel Drug Delivery Research Group.

References

1 D. Nandi, M. Debnath, J. Forster, A. Pandey, H. Bharadwaj and R. Patel, *et al.*, Nanoparticle-mediated co-delivery of inflammasome inhibitors provides protection against sepsis, *Nanoscale*, 2024, **16**(9), 4678–4690.
2 L. J. Schlapbach, N. Kissoon, A. Alhawsawi, M. H. Aljuaid, R. Daniels and L. A. Gorordo-Delsol, *et al.*, World Sepsis Day: a global agenda to target a leading cause of morbidity and mortality, *Am. J. Physiol.: Lung Cell. Mol. Physiol.*, 2020, **319**(3), L518–L522.
3 A. Cassini, B. Allegranzi, C. Fleischmann-Struzek, T. Kortz, R. Markwart and H. Saito, *et al.*, *Global report on the epidemiology and burden on sepsis: current evidence, identifying gaps and future directions*, World Health Organization, 2020.
4 WHO, Report signals increasing resistance to antibiotics in bacterial infections in humans and need for better data: World Health Organization, 2022 [Available from: https://www.who.int/news/item/09-12-2022-report-signals-increasing-resistance-to-antibiotics-in-bacterial-infections-in-humans-and-need-for-better-data#:~:text=A%20new%20World%20Health%20Organization,by%2087%20countries%20in%202020].
5 A. Pant, I. Mackraj and T. Govender, Advances in sepsis diagnosis and management: a paradigm shift towards nanotechnology, *J. Biomed. Sci.*, 2021, **28**(1), 6.
6 Y. Zhao, M. Pu, J. Zhang, Y. Wang, X. Yan and L. Yu, *et al.*, Recent advancements of nanomaterial-based therapeutic strategies toward sepsis: bacterial eradication, anti-inflammation, and immunomodulation, *Nanoscale*, 2021, **13**(24), 10726–10747.
7 M. A. Gafar, C. A. Omolo, E. Elhassan, U. H. Ibrahim and T. Govender, Applications of peptides in nanosystems for diagnosing and managing bacterial sepsis, *J. Biomed. Sci.*, 2024, **31**(1), 40.
8 A. Tageldin, C. A. Omolo, V. O. Nyandoro, E. Elhassan, S. Z. F. Kassam and X. Q. Peters, *et al.*, Engineering dynamic covalent bond-based nanosystems for delivery of antimicrobials against bacterial infections, *J. Controlled Release*, 2024, **371**, 237–257.
9 M. A. Gafar, C. A. Omolo, U. H. Ibrahim, X. Q. Peters, E. A. Ismail and R. Khan, *et al.*, Antimicrobial peptide-fucoidan nanoplexes: a novel multifunctional biomimetic nanocarrier for enhanced vancomycin delivery against bacterial infections and sepsis, *Int. J. Pharm.*, 2025, **672**, 125344.
10 C. Y. Zhang, J. Gao and Z. Wang, Bioresponsive nanoparticles targeted to infectious microenvironments for sepsis management, *Adv. Mater.*, 2018, **30**(43), 1803618.
11 M. A. Gafar, C. A. Omolo, U. H. Ibrahim, G. Elamin, A. Tageldin and E. Elhassan, *et al.*, Hyaluronic acid-silybin conjugate for the preparation of multifunctional, biomimetic, vancomycin-loaded self-assembled polymersomes against bacterial sepsis, *Int. J. Biol. Macromol.*, 2025, **299**, 140152.
12 U. H. Ibrahim, N. Devnarain and T. Govender, Biomimetic strategies for enhancing synthesis and delivery of

antibacterial nanosystems, *Int. J. Pharm.*, 2021, **596**, 120276.
13 B. Chen, F. Li, X. K. Zhu, W. Xie, X. Hu and M. H. Zan, *et al.*, Highly biocompatible and recyclable biomimetic nanoparticles for antibiotic-resistant bacteria infection, *Biomater. Sci.*, 2021, **9**(3), 826–834.
14 N. Jan, A. Madni, S. Khan, H. Shah, F. Akram and A. Khan, *et al.*, Biomimetic cell membrane-coated poly(lactic-*co*-glycolic acid) nanoparticles for biomedical applications, *Bioeng. Transl. Med.*, 2023, **8**(2), e10441.
15 Y. Wang, L. Liu, X. Zheng and X. Liu, Membrane-camouflaged biomimetic nanoparticles as potential immunomodulatory solutions for sepsis: an overview, *Front. Bioeng. Biotechnol.*, 2023, **11**, 1111963.
16 E. A. D. Ezekwe, C. Weng and J. A. Duncan, ADAM10 Cell surface expression but not activity is critical for Staphylococcus aureus α-hemolysin-mediated activation of the NLRP3 inflammasome in human monocytes, *Toxins*, 2016, **8**(4), 95.
17 S. Krivan, A. Kapelouzou, S. Vagios, D. I. Tsilimigras, M. Katsimpoulas and D. Moris, *et al.*, Increased expression of Toll-like receptors 2, 3, 4 and 7 mRNA in the kidney and intestine of a septic mouse model, *Sci. Rep.*, 2019, **9**(1), 4010.
18 S. Liao, Y. Lin, L. Liu, S. Yang, Y. Lin and J. He, *et al.*, ADAM10-a ''multitasker'' in sepsis: focus on its posttranslational target, *Inflammation Res.*, 2023, **72**(3), 395–423.
19 E. Elhassan, C. A. Omolo, M. A. Gafar, E. A. Ismail, U. H. Ibrahim and R. Khan, *et al.*, Multifunctional hyaluronic acid-based biomimetic/pH-responsive hybrid nanostructured lipid carriers for treating bacterial sepsis, *J. Biomed. Sci.*, 2025, **32**(1), 19.
20 J. Guo, Y. Miao, F. Nie, F. Gao, H. Li and Y. Wang, *et al.*, Zn-Shik-PEG nanoparticles alleviate inflammation and multi-organ damage in sepsis, *J. Nanobiotechnol.*, 2023, **21**(1), 448.
21 S. Wang, Y. Chen, S. Han, Y. Liu, J. Gao and Y. Huang, *et al.*, Selenium nanoparticles alleviate ischemia reperfusion injury-induced acute kidney injury by modulating GPx-1/NLRP3/Caspase-1 pathway, *Theranostics*, 2022, **12**(8), 3882–3895.
22 E. Elhassan, N. Devnarain, M. Mohammed, T. Govender and C. A. Omolo, Engineering hybrid nanosystems for efficient and targeted delivery against bacterial infections, *J. Controlled Release*, 2022, **351**, 598–622.
23 F. Persano, G. Gigli and S. Leporatti, Lipid–polymer hybrid nanoparticles in cancer therapy: current overview and future directions, *Nano Express*, 2021, **2**(1), 012006.
24 V. Dave, K. Tak, A. Sohgaura, A. Gupta, V. Sadhu and K. R. Reddy, Lipid–polymer hybrid nanoparticles: synthesis strategies and biomedical applications, *J. Microbiol. Methods*, 2019, **160**, 130–142.
25 E. Elhassan, C. A. Omolo, M. A. Gafar, L. W. Kiruri, U. H. Ibrahim and E. A. Ismail, *et al.*, Disease-Inspired design of biomimetic tannic acid–based hybrid nanocarriers for enhancing the treatment of bacterial-induced sepsis, *Mol. Pharmaceutics*, 2024, **21**(10), 4924–4946.
26 F. Oppedisano, R. Macrì, M. Gliozzi, V. Musolino, C. Carresi and J. Maiuolo, *et al.*, The anti-inflammatory and antioxidant properties of n-3 PUFAs: their role in cardiovascular protection, *Biomedicines.*, 2020, **8**(9), 306.
27 D. Dipasquale, L. Basiricò, P. Morera, R. Primi, A. Tröscher and U. Bernabucci, Anti-inflammatory effects of conjugated linoleic acid isomers and essential fatty acids in bovine mammary epithelial cells, *Animal*, 2018, **12**(10), 2108–2114.
28 G. Zhao, T. D. Etherton, K. R. Martin, J. P. Vanden Heuvel, P. J. Gillies and S. G. West, *et al.*, Anti-inflammatory effects of polyunsaturated fatty acids in THP-1 cells, *Biochem. Biophys. Res. Commun.*, 2005, **336**(3), 909–917.
29 M. Zhou, W. Jiang, J. Xie, W. Zhang, Z. Ji and J. Zou, *et al.*, Peptide-mimicking poly(2-oxazoline)s displaying Potent antimicrobial properties, *ChemMedChem*, 2021, **16**(2), 309–315.
30 P. C. Appelbaum, The emergence of vancomycin-intermediate and vancomycin-resistant Staphylococcus aureus, *Clin. Microbiol. Infect.*, 2006, **12**(s1), 16–23.
31 H. M. Berman, T. Battistuz, T. N. Bhat, W. F. Bluhm, P. E. Bourne and K. Burkhardt, *et al.*, The protein data bank, *Biol. Crystallogr.*, 2002, **58**(6), 899–907.
32 M. D. Hanwell, D. E. Curtis, D. C. Lonie, T. Vandermeersch, E. Zurek and G. R. Hutchison, Avogadro: an advanced semantic chemical editor, visualization, and analysis platform, *J. Cheminf.*, 2012, **4**(1), 17.
33 C. Dominguez, R. Boelens and A. M. J. J. Bonvin, HADDOCK: a protein–protein docking approach based on biochemical or biophysical information, *J. Am. Chem. Soc.*, 2003, **125**(7), 1731–1737.
34 R. V. Honorato, M. E. Trellet, B. Jiménez-García, J. J. Schaarschmidt, M. Giulini and V. Reys, *et al.*, The HADDOCK2.4 web server for integrative modeling of biomolecular complexes, *Nat. Protoc.*, 2024, **19**(11), 3219–3241.
35 E. F. Pettersen, T. D. Goddard, C. C. Huang, G. S. Couch, D. M. Greenblatt and E. C. Meng, *et al.*, UCSF Chimera—A visualization system for exploratory research and analysis, *J. Comput. Chem.*, 2004, **25**(13), 1605–1612.
36 W. L. DeLano, *The PyMOL molecular graphics system*, 2002, https://www.pymolorg/.
37 A. C. Wallace, R. A. Laskowski and J. M. Thornton, LIGPLOT: a program to generate schematic diagrams of protein-ligand interactions, *Protein Eng.*, 1995, **8**(2), 127–134.
38 H. Elkateb, L. M. Tatham, H. Cauldbeck, E. Niezabitowska, A. Owen and S. Rannard, *et al.*, Optimization of the synthetic parameters of lipid polymer hybrid nanoparticles dual loaded with darunavir and ritonavir for the treatment of HIV, *Int. J. Pharm.*, 2020, **588**, 119794.
39 E. A. Ismail, C. A. Omolo, M. A. Gafar, R. Khan, V. O. Nyandoro and E. Y. Salifu, *et al.*, Multi-functional pH-responsive and biomimetic chitosan-based nanoplexes for targeted delivery of ciprofloxacin against bacterial sepsis, *Int. J. Biol. Macromol.*, 2024, **262**, 130046.
40 Y. Zhang, M. Huo, J. Zhou, A. Zou, W. Li and C. Yao, *et al.*, DDSolver: an add-in program for modeling and comparison of drug dissolution profiles. The, *AAPS J.*, 2010, **12**(3), 263–271.

41 J. H. Jorgensen and J. D. Turnidge, Susceptibility test methods: dilution and disk diffusion methods, *Man. Clin. Microbiol.*, 2015, 1253–1273.
42 E. A. Ismail, C. A. Omolo, M. A. Gafar, R. Khan, V. O. Nyandoro and E. S. Yakubu, *et al.*, Novel peptide and hyaluronic acid coated biomimetic liposomes for targeting bacterial infections and sepsis, *Int. J. Pharm.*, 2024, **662**, 124493.
43 W. Zhan, L. Xin, L. Lianghe, C. Zhongsheng, T. Tian and Y. Lei, *et al.*, In vitro mitochondrial-targeted antioxidant peptide induces apoptosis in cancer cells, *OncoTargets Ther.*, 2019, **12**, 7297–7306.
44 C. Zhan, G. Lin, Y. Huang, Z. Wang, F. Zeng and S. Wu, A dopamine-precursor-based nanoprodrug for in-situ drug release and treatment of acute liver failure by inhibiting NLRP3 inflammasome and facilitating liver regeneration, *Biomaterials*, 2021, **268**, 120573.
45 E. A. Ismail, V. O. Nyandoro, C. A. Omolo and T. Govender, Nanocarrier-based targeting of pattern recognition receptors as an innovative strategy for enhancing sepsis therapy. Advanced Healthcare, *Materials*, 2025, **14**(23), 2501146.
46 S. El Deeb, A. Al-Harrasi, A. Khan, M. Al-Broumi, G. Al-Thani and M. Alomairi, *et al.*, Microscale thermophoresis as a powerful growing analytical technique for the investigation of biomolecular interaction and the determination of binding parameters, *Methods Appl. Fluoresc.*, 2022, **10**(4), 042001.
47 L. Huang and C. Zhang, Microscale thermophoresis (MST) to detect the interaction between purified proteins and small molecules, in *Plant Chemical Genomics: Methods and Protocols*, ed. G. R. Hicks and C. Zhang, Springer US, New York, NY, 2021, pp. 187–193.
48 S. A. I. Seidel, P. M. Dijkman, W. A. Lea, G. van den Bogaart, M. Jerabek-Willemsen and A. Lazic, *et al.*, Microscale thermophoresis quantifies biomolecular interactions under previously challenging conditions, *Methods*, 2013, **59**(3), 301–315.
49 P. Ahmaditabar, A. A. Momtazi-Borojeni, A. H. Rezayan, M. Mahmoodi, A. Sahebkar and M. Mellat, Enhanced entrapment and improved in vitro controlled release of *N*-acetyl cysteine in hybrid PLGA/lecithin nanoparticles prepared using a nanoprecipitation/self-assembly method, *J. Cell. Biochem.*, 2017, **118**(12), 4203–4209.
50 O. Koshy, L. Subramanian and S. Thomas, Differential scanning calorimetry in nanoscience and nanotechnology, in *Thermal and Rheological Measurement Techniques for Nanomaterials Characterization*, ed. S. Thomas, R. Thomas, A. K. Zachariah and R. K. Mishra, Elsevier, 2017, ch. 5, pp. 109–122.
51 B. T. Raimi-Abraham, J. G. Moffat, P. S. Belton, S. A. Barker and D. Q. M. Craig, Generation and characterization of standardized forms of trehalose dihydrate and their associated solid-state behavior, *Cryst. Growth Des.*, 2014, **14**(10), 4955–4967.
52 H. B. Mohamed, S. M. El-Shanawany, M. A. Hamad and M. Elsabahy, Niosomes: a strategy toward prevention of clinically significant drug incompatibilities, *Sci. Rep.*, 2017, **7**(1), 6340.
53 Z. Zhang, R. M. Elkanayati, S. Feng, I. Karnik, S. K. Vemula and M. A. Repka, Investigating the potential of poly(2-ethyl-2-oxazoline) and its polymer blends for enhancing fenofibrate amorphous solid dispersion dissolution profile, *Pharmaceutics*, 2025, **17**(10), 1238.
54 H. Su, Y. Wang, Y. Gu, L. Bowman, J. Zhao and M. Ding, Potential applications and human biosafety of nanomaterials used in nanomedicine, *J. Appl. Toxicol.*, 2018, **38**(1), 3–24.
55 Standardization IOf. Biological evaluation of medical devices – part 5: tests for in vitro cytotoxicity International Organization for Standardization: International Organization for Standardization, 2018 [Available from: https://www.iso.org/standard/68936.html].
56 T. R. Kyriakides, A. Raj, T. H. Tseng, H. Xiao, R. Nguyen and F. S. Mohammed, *et al.*, Biocompatibility of nanomaterials and their immunological properties, *Biomed. Mater.*, 2021, **16**(4), 042005.
57 R. A. Peterfreund and J. H. Philip, Critical parameters in drug delivery by intravenous infusion, *Expert Opin. Drug Delivery*, 2013, **10**(8), 1095–1108.
58 N. Seedat, R. S. Kalhapure, C. Mocktar, S. Vepuri, M. Jadhav and M. Soliman, *et al.*, Co-encapsulation of multi-lipids and polymers enhances the performance of vancomycin in lipid–polymer hybrid nanoparticles: in vitro and in silico studies, *Mater. Sci. Eng., C*, 2016, **61**, 616–630.
59 V. Papadopoulou, K. Kosmidis, M. Vlachou and P. Macheras, On the use of the Weibull function for the discernment of drug release mechanisms, *Int. J. Pharm.*, 2006, **309**(1), 44–50.
60 S. J. Sonawane, R. S. Kalhapure, S. Rambharose, C. Mocktar, S. B. Vepuri and M. Soliman, *et al.*, Ultra-small lipid-dendrimer hybrid nanoparticles as a promising strategy for antibiotic delivery: in vitro and in silico studies, *Int. J. Pharm.*, 2016, **504**(1), 1–10.
61 N. Osman, C. A. Omolo, M. A. Gafar, N. Devnarain, S. Rambharose and U. H. Ibrahim, *et al.*, Niosomes modified with a novel pH-responsive coating (mPEG-OA) enhance the antibacterial and anti-biofilm activity of vancomycin against methicillin-resistant Staphylococcus aureus, *Nano Express*, 2024, **5**(1), 015008.
62 J. C. Nwabuife, D. Hassan, A. Madhaorao Pant, N. Devnarain, M. A. Gafar and N. Osman, *et al.*, Novel vancomycin free base – Sterosomes for combating diseases caused by Staphylococcus aureus and Methicillin-resistant Staphylococcus aureus infections (S. Aureus and MRSA), *J. Drug Delivery Sci. Technol.*, 2023, **79**, 104089.
63 V. O. Nyandoro, C. A. Omolo, E. A. Ismail, L. Yong and T. Govender, Inflammation-responsive drug delivery nanosystems for treatment of bacterial-induced sepsis, *Int. J. Pharm.*, 2023, **644**, 123346.
64 D. Qin, W. Hu, Y. Guo, R. Cheng, F. Hao and B. Zhao, Baicalein based nano-delivery system restores mitochondrial homeostasis through PPAR signaling pathway to

promote wound healing in diabetes, *J. Nanobiotechnol.*, 2025, **23**(1), 360.
65 L. Lu, L. Quan, J. Li, J. Yuan, X. Nie and X. Huang, *et al.*, Bioengineered stem cell membrane functionalized nanoparticles combine anti-inflammatory and antimicrobial properties for sepsis treatment, *J. Nanobiotechnol.*, 2023, **21**(1), 170.
66 T. Li, Y. Qian, Z. Miao, P. Zheng, T. Shi and X. Jiang, *et al.*, Xuebijing injection alleviates Pam3CSK4-induced inflammatory response and protects mice from sepsis caused by methicillin-sesistant Staphylococcus aureus, *Front. Pharm.*, 2020, **11**, 104.
67 C. Nedeva, Inflammation and cell death of the innate and adaptive immune system during sepsis, *Biomolecules*, 2021, **11**(7), 1011.
68 C.-C. Liao, H.-P. Yu, S.-C. Yang, A. Alalaiwe, Y.-S. Dai and F.-C. Liu, *et al.*, Multifunctional lipid-based nanocarriers with antibacterial and anti-inflammatory activities for treating MRSA bacteremia in mice, *J. Nanobiotechnol.*, 2021, **19**(1), 48.